Master Thesis

Development of a Sand Prediction Model for a Gas Field Located in South Tunisia

Written by:
Mouhamed Abdellatif, BSc
1435461

Advisor:
Univ.-Prof. Dipl.-Ing. Dr.mont. Herbert Hofstätter

Leoben, 24.11.2017

EIDESSTATTLICHE ERKLÄRUNG

Ich erkläre an Eides statt, dass ich die vorliegende Diplomarbeit selbständig und ohne fremde Hilfe verfasst, andere als die angegebenen Quellen und Hilfsmittel nicht benutzt und die den benutzten Quellen wörtlich und inhaltlich entnommenen Stellen als solche erkenntlich gemacht habe.

AFFIDAVIT

I hereby declare that the content of this work is my own composition and has not been submitted previously for any higher degree. All extracts have been distinguished using quoted references and all information sources have been acknowledged.

Danksagung / Acknowledgement

My appreciation goes to OMV for giving me the opportunity to pursue this degree. I would like to express my deepest appreciation to Mr. David Simpson, technical advisor sand control at OMV, and Mr. Robert Maier, lead engineer at OMV, for their insights and suggestions. My deepest thanks go to Mr. Chahine Bahri, production manager in OMV Tunisia, for his support and continued encouragement during my internship.

I wish to express my gratitude to my supervisor, Prof. Herbert Hofstätter for his guidance and support. I also benefited a lot from many courses taught by him. I would like to thank Mr. Abbas Zamani and Ms. Fatima Fazeli for their continued encouragement and valuable suggestions during this work. I would like to express my deepest thanks to my friend Ghassen Yahyaoui who has helped me with implementing the model in the VBA.

Finally, I must express my very profound gratitude to my parents for providing me with unfailing support and continuous encouragement throughout my years of study and through the process of writing this thesis. This accomplishment would not have been possible without them.

Kurzfassung

Die Förderung von Sand ist ein großes Problem in vielen Gas- und Ölfeldern weltweit. Die Ursachen sind die Anwesenheit von desintegriertem Sand im bohrlochnahem Bereich sowie durchgeführte Perforationsarbeiten. Um eine effektive Strategie zur Sandbehandlung zu finden, ist es notwendig die Produktionsverhältnisse vorauszuberechnen welche möglicherweise zu technischem Versagen in Verbindung mit Sand führen.

Das Ziel dieser Arbeit ist es ein analytischen Sandvorhersagemodell für ein Gasfeld im Süden Tunesiens zu erstellen, welches Ingenieure im Entscheidungsprozess unterstützt und ihnen ermöglicht kritische Bohrlochdrücke und Zustände zu erkennen um Sandproduktion zu vermeiden. Das Vorhersagemodell ist eine analytische Lösung basierend auf dynamischen Gesteinsparametern, welche durch Bohrlochmessung bestimmt und mit Hilfe des Sandproduktionskriteriums nach Wilson et al. weiter verwendet wurden. Da die vorgestellte Methode mit durch Bohrlochmessung erhobenen Daten arbeitet, kann das Modell schnell und kostengünstig zur Vorhersage implementiert werden und zukünftige Probleme verbunden mit der Förderung von Sand verhindern.

Das Modell wurde in Microsoft Excel implementiert und mit Hilfe von Visual Basic entwickelt, welches ein benutzerfreundliches Interface vorweist. Das Modell wurde mit Daten von drei verschiedenen Gasproduktionssonden welche Sandproduktion aufweisen getestet und evaluiert. Die berechneten Ergebnisse zeigen, dass Sandproduktion erfolgreich und frühzeitig vorhergesagt werden kann und somit rechtzeitig Maßnahmen ergriffen werden können

Abstract

Sand production is a major problem in many fields worldwide resulting from the presence of the disintegrated grain around the wellbore and/or the perforation. In order to develop the effective sand management strategy, it is necessary to predict the production condition that may lead to the sanding failure.

The purpose of this study is to build an analytical sand prediction model for a gas field located in the south of Tunisia which could assist the engineer to make better decisions by estimating the critical well pressure below which sand production is expected. The prediction scheme is an analytical solution based on dynamic mechanical rock properties determined from well-logging data utilizing the sand production criterion described by Wilson et al. Being based on well logging data, the model is a quick, low cost, first-hand prediction method that can be implemented to avoid the potentially serious problems associated with sand production.

The model was implemented in Microsoft Excel by using Visual Basic which provides a user-friendly interface and it was validated using field data gathered from three gas wells that have shown sand production during testing. The model-generated results of the three wells successfully matched the sand production during testing and they indicate the likelihood of sand production at an early stage of production.

List of Tables

List of Figures

Abbreviations

Variable	Meaning	Units
A	Poro-Elastic Constant	ratio
Bf	Boost Factor	–
$BHFP$	Bottomhole Flowing Pressure	psi
$CBHFP$	Critical Bottomhole Flowing Pressure	psi
$DTCO$	Compressional Wave travel Time	$\mu s/ft$
$DTSH$	Shear Wave travel Time	$\mu s/ft$
E_{dyn}	Dynamic Young's modulus	psi
E_{Sta}	Static Young's modulus	psi
F	Failure Function	–
FIT	Formation Integrity Test	–
G_{dyn}	Dynamic Shear Modulus	psi
HCS	Hole-Collapse Strength	–
I_{sh}	Shaliness Index	–
J_1	First Invariant of Stress Tensor	psi
J_2	Second Invariant of Stress Tensor	psi^2
K_{dyn}	Dynamic Bulk Modulus	psi
LOT	Leak Off Test	–
m_h	Material Constant	–
Mw	Mud Weight	ppg
p_{pn}	Normal Pore Pressure	psi
p_p	Pore Pressure	psi

p_r	Reservoir Pressure	psi
p_w	Wellbore Pressure	psi
S_L	Material Constant	
TWC	Thick Hollow Cylinder	$-$
V_P	Compressional Wave Velocity	m/s
Z	Depth	ft
ρ_b	Bulk Density	g/cc
α	Biot's Coefficient	$-$
α_{perf}	Perforation Angle	deg
$\emptyset$	Porosity	$-$
$\emptyset_f$	Frictional Angle	deg
η_L	Material Constant	$-$
$\vartheta_{dyn}, \mu_{dyn}$	Dynamic Poisson's Ratio	$-$
μ_{sta}	Static Poisson's Ratio	$-$
σ_1	Maximum Principle Stress	psi
σ_2	Intermediate Principle Stress	psi
σ_3	Minimum Principle Stress	psi
σ_v	Vertical Stress	psi
$\sigma_{H\,max}$	Maximum Horizontal Stress	psi
$\sigma_{h\,min}$	Minimum Horizontal Stress	psi
σ_n	Normal Stress	psi
σ_{tmax}	Maximum Principle Tangential Stress	psi
σ_{tmin}	Minimum Principle Tangential Stress	psi

$\sigma_{tmax,eff}$	Maximum Effective Tangential Compressive Stress	psi
τ	Shear Stress	psi
Δt_s	Compressional Wave Travel Time	$\mu s/ft$
Δt_C	Shear Wave Travel Time	$\mu s/ft$

Table of content

Page

1 Introduction

1.1 Problem Description

Over 70% of world's oil and gas reserves are contained in sand formations where sand production is likely to become a problem during the life of the well. Formation sand produced with formation fluid can erode downhole and surface equipment as well as causing formation collapse and block surface flow lines. This has prompted the continued search for solutions to mitigate sand production in the oil and gas industry.

Screens and gravel packs are the most widely sand control treatments used to prevent sand flowing into the wellbore. Nevertheless, their initial installation costs are generally high and they are not free from problems. In fact, Screen systems come with a risk of failure [27].

Utilizing sand control measure like gravel pack when it is not needed is an unnecessary expense and can reduce production rates. Conversely, if sanding occurs and no sand control is implemented, potential problems associated with sand production can occur such as erosion to surface and downhole facilities, casing collapse and lost production time due to shut in of the well, to change equipment or clean the sand filled wellbore. Therefore, a sand production prediction study is of great interest for the operator to estimate the sand potential of the field within its lifespan.

1.2 Field Background

The targeted reservoirs are the Silurian sandstones of the Acacus formation located approximately at 3700 m TVD and the second target is the uppermost Tannezuft formation (approximately 3900 m TVD).

The Acacus formation is subdivided into three units from top to bottom C, B and A, (figure 1). The top unit, Acacus C, has an average thickness of 100m, and is the shallowest and youngest unit. This unit is dominated by claystone interbedded with siltstone and some sandstone layers. The next unit is the Acacus B with an average thickness of 100 m and is dominated by claystone with some silt and sandstone. The deepest and oldest unit which has an average thickness of 252 m is the Acacus A. This unit consists mainly of sandstone interbedded with claystone acting as intra-formational seals [1].

The uppermost Tannezuft formation consists of grey to dark grey claystone interbedded with few sandstone and siltstone layers. The thickness of the reservoir sandstones does not exceed 20m and high-quality sandstones are only present in the uppermost 100m of the formation [1].

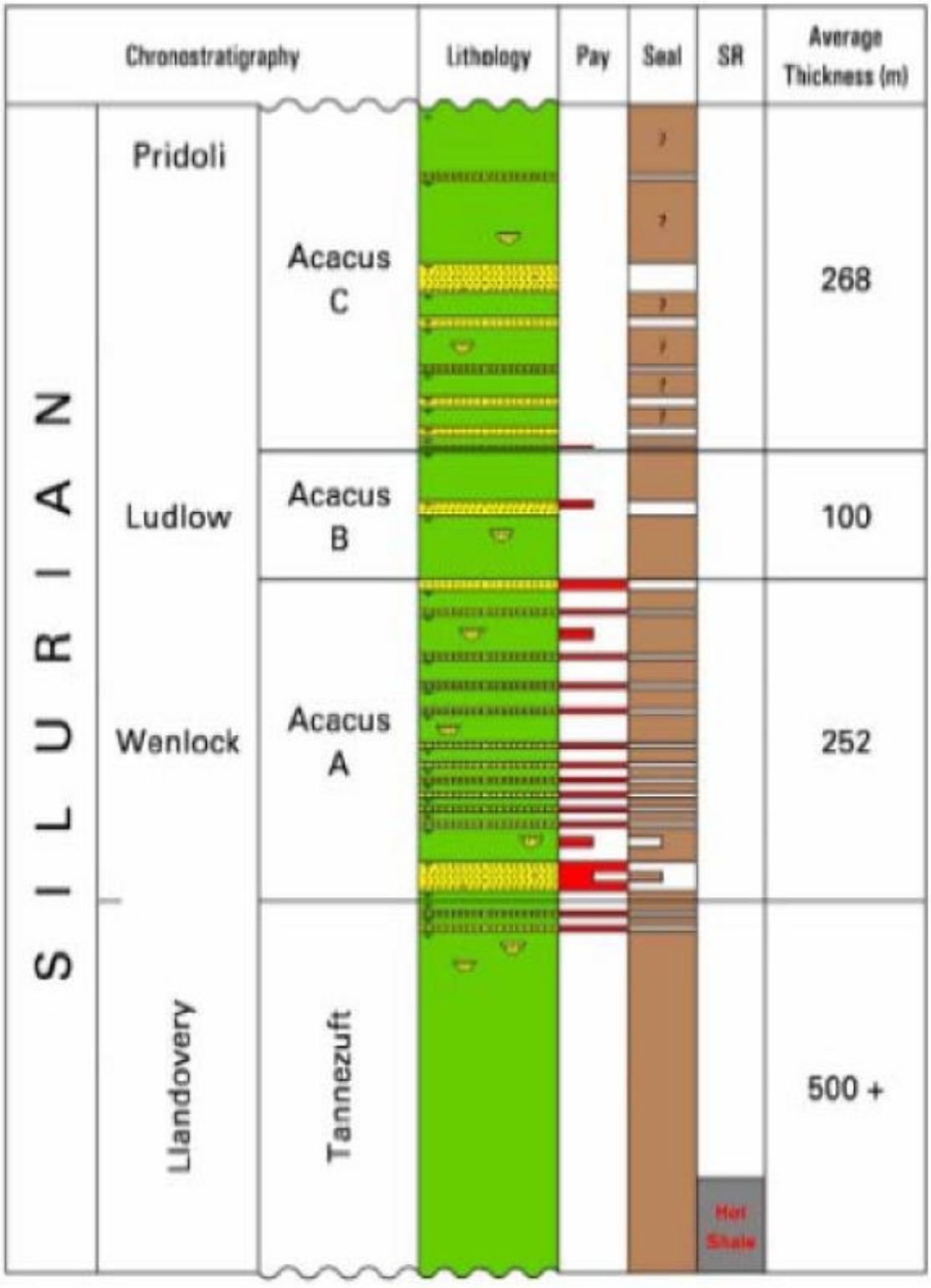

Figure 1: Lithology Column for the Field [1]

The porosity and the permeability of this field range from 11 to 30% and from 0.1 to 336 mD respectively. The predominant porosity types are reduced intergranular porosity and the micro-porosity of iron chlorite cements [1].

There are 11 wells were drilled in this field. According to the structure of the reservoir, the wells are designed to be vertical with a 7” production liner across the zone of interest. During the testing of the wells, sand production was noted in some of the 11 wells.

1.3 Objectives

The aim of this study was to develop an analytical sand prediction model by using excel for the gas field located in south of Tunisia. The purpose of this model is to estimate the critical wellbore pressure below which sanding is expected. In order to have quick and reasonable estimates of sanding problem prior to completion, this model uses mechanical properties calculated from well logging data which are representative for individual wellbore conditions. It’s a quick first-hand sand prediction method that can be implemented once the well is drilled and before completion.

1.4 Thesis Outline

The thesis is divided into six chapters. The current chapter, chapter 1, provides the background and the objectives of this study. The second chapter reviews some rock mechanics concepts relevant to the sand production problem. In addition, the literature from past work on sand prediction models is briefly described.

In the third chapter, the methodology used to calculate the geomechanical properties from well logging data is explained. The fourth chapter describes the sand failure criterion and related stress transformation around the wellbore. The results obtained from the sand production evaluation of the study wells are summarized in the fifth chapter. Finally, the sixth chapter is the conclusion of the study.

2 Literature Review and Theory

Sand production is the production of small or large amounts of sand together with the reservoir fluids. The sand production is usually given in petroleum engineering in pounds per thousand barrels (pptb). The process of the sand production is divided into the following three main stages. The first stage is the loss of mechanical integrity of the rocks surrounding an open hole or perforation. The second stage is the separation of the solid particles from the rocks. Final stage is the transportation of the solid particles to the surface by reservoir fluids. Sand production is a complex phenomenon that is dependent on the stresses near a wellbore and the geomechanical properties of the reservoir rocks. Therefore, to accurately predict sand production potential, knowledge of the formation´s mechanical strength, the in-situ stresses and rock failure mechanism is required [2].

This chapter reviews the main essential literatures regarding sand production prediction and related rock failure criteria. In addition, the essential geomechanical properties will be explained.

2.1 Rock Mechanical Properties

The rock mechanical properties mainly include Young's modulus, Poisson's ratio and rock strength. These parameters can be obtained by lab experiments of core samples. When the rock samples are not available, the well log data and geophysical data can be used to generate the rock mechanical properties.

2.1.1 Stress

The stress is defined as the force acting over a given area [3]. Stresses have both magnitudes and orientation. The SI unit for stress is Pascal (Pa = N/m2). In the petroleum industry, pounds per square inch (psi) is extensively used.

$$Stress = \sigma = \frac{F(Force)}{A(Area)} \tag{2.1}$$

The stress on a plane is divided into two components, one perpendicular to the plane face, the normal stress (σ), and the other parallel to the plane, the shear stress (σ_{xy}). For a given point, P, in the surface, stress is defined in terms of three normal stresses and six shear stresses. All the nine stress components related to the point P is expressed in the form of a stress tensor:

$$P = \begin{bmatrix} \sigma_x & \sigma_{xy} & \sigma_{xz} \\ \sigma_{yx} & \sigma_y & \sigma_{yz} \\ \sigma_z & \sigma_{zy} & \sigma_z \end{bmatrix} \tag{2.2}$$

2.1.2 Strain

Strain, ε, is the change in length per original length due to an applied load. The fundamental relation between stress and strain is described by Hooke's law:

$$\sigma = E.\varepsilon \tag{2.3}$$

Where, E is the Young's modulus.

2.1.3 Effective Stress

The concept of the effective stress is introduced by Terzaghi (1923) [3]. It is defined as

$$\sigma_{ij} = S_{ij} - \delta_{ij}\alpha p_f \tag{2.4}$$

Where, δ_{ij} is the Kronecker symbol, α is called the Biot coefficient or the effective stress coefficient, S_{ij} is the total external stress and p_f is the pore pressure.

This equation, Eq 2.4, indicates that the effective stress is the difference between externally stresses and internal pore pressure. Which means that the total external stress S_{ij}, is not carried only by the grains, which carries the part σ_{ij} but also by the fluid, which carries the remaining part αp_f.

The Biot coefficient is defined as

$$\alpha = 1 - \frac{K_b}{K_g} \tag{2.5}$$

Where, $\mathrm{K_b}$ is drained bulk modulus and $\mathrm{K_g}$ is the bulk modulus of the rock's individual solid grains. The Biot coefficient is restricted to the region $0 \leq \alpha \leq 1$. In unconsolidated or weak sandstones, α is close to 1.

2.1.4 Young's Modulus

The Young's modulus, E, is an important parameter to describe stress and strain relationship. It is a measure of the stiffness of a material and it is applicable to a linear elastic region where stress is directly proportional to strain, figure 2. The Young's modulus is expressed by:

$$\sigma = E\varepsilon \tag{2.6}$$

Where, σ is the stress and, ε is the strain.

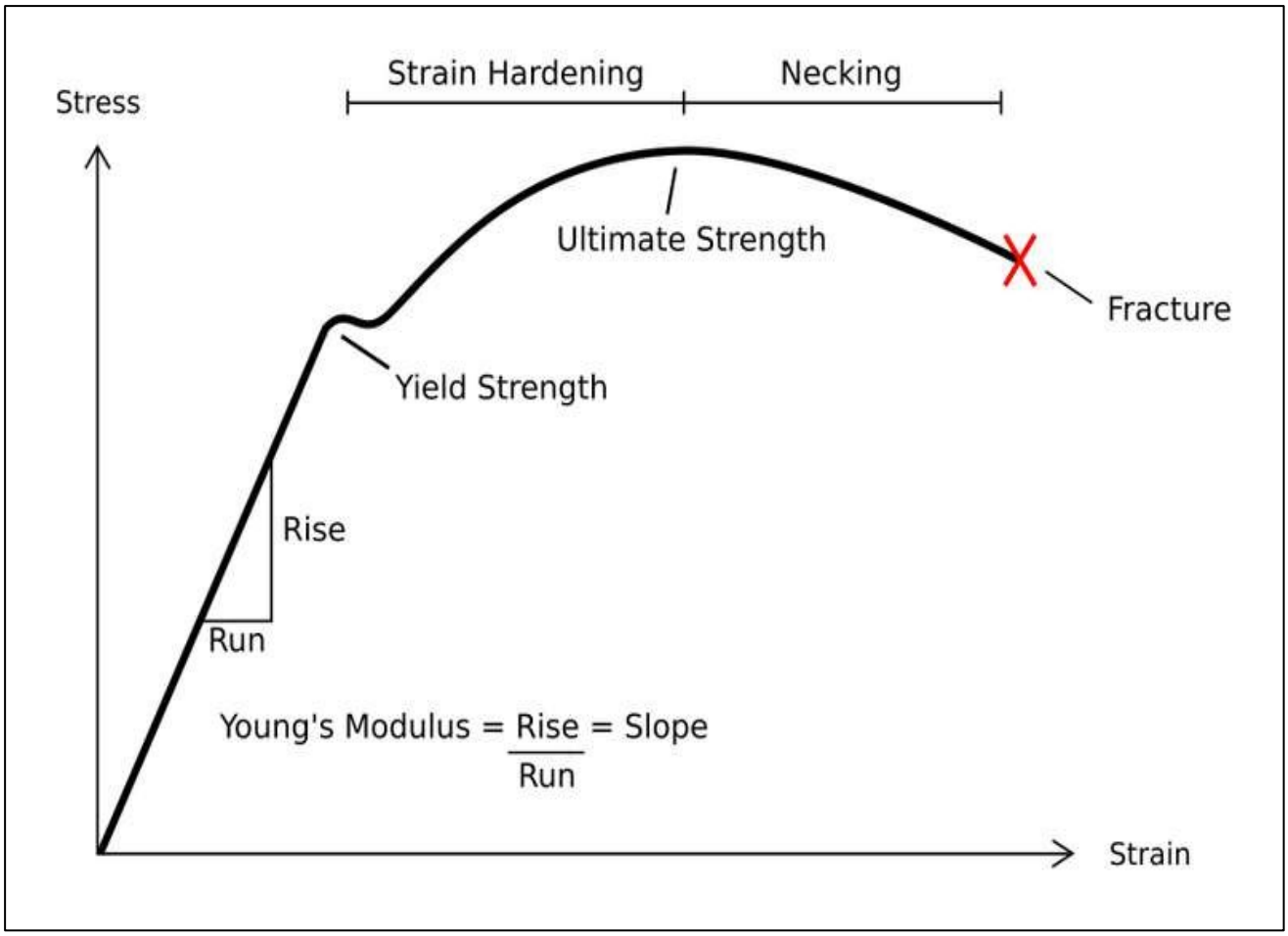

Figure 2: Young's Modulus and Stress-Strain Curve.

2.1.5 Poisson's Ratio

Poisson's ratio is the ratio of transverse strain to corresponding axial strain on a material stressed along one axis. For a rock core subjected to axial load, Poisson's ratio, ϑ, can be expressed as:

$$\vartheta = -\frac{\varepsilon_L}{\varepsilon_a} \tag{2.7}$$

Where, ε_L is the lateral strain and ε_a is the axial strain. Therefore, Poisson's ratio can be determined by measuring the lateral and axial deformations of the uniaxial compressive test in rock samples.

2.2 Sand Production

Sand production may start from the moment a well is first produced or at some later time during production. The sand production rate may decrease, in the best case, if a natural filter is created by sand grains arching around the perforation and reducing the flow of sand grains into the well. However, the sand production may continue or even increase. In the worst case, this may result in the well sanding-up and ceasing production.

In most cases sand production will continue unless some sand control method is employed. Controlling sand production can be achieved by completing the well with an active sand control technique or through the application of reservoir engineering principles.

Active sand control techniques are mechanical or chemical measures used to hold the formation in place. The most common means are gravel packs, sand screens and chemical consolidation.

In the reservoir engineering approach, a well is completed naturally, without any active sand control devises, and special precautions are outlined to avoid or control the sanding problem. The reservoir engineering approach is based on field observation of factors associated with sand production as well as the rock-mechanical analysis of the stresses causing instability of the wellbore. These observations are used to limit the production rate and the pressure drawdown to control the flow of the sand.

The key to controlling the sanding problem by either approach is effectively predicting sand production before the well is completed. Predicting the onset of sanding is a broad geomechanical issue which has been the subject of many studies for decades. Several models have been published to analyze and predict the condition under which wells start producing sand. Sanding prediction models are generally regrouped in either analytical or numerical models.

Regardless of the category of the predictive models, the sanding onset prediction is based on the arch, perforation tunnel or borehole instability. Generally, a stress model is established to obtain the stress state near the sand arch, perforation tunnel or borehole, and then a sand production criterion is applied in order to predict the production conditions at which sand production occurs.

2.2.1 Sand Prediction Models

The role of arching in sand stability was first treated by Terzaghi (1936) [4] in his trap door experiment, which demonstrated that arching was a real and stable phenomenon. Hall and Harrisberger (1970) [5] introduced the principle of arching in sand stability in the oil industry. The sand arch, figure 3, was defined as “a curved structure spanning an opening, serving to support a load by resolving the vertical stress into horizontal stresses “ [5]

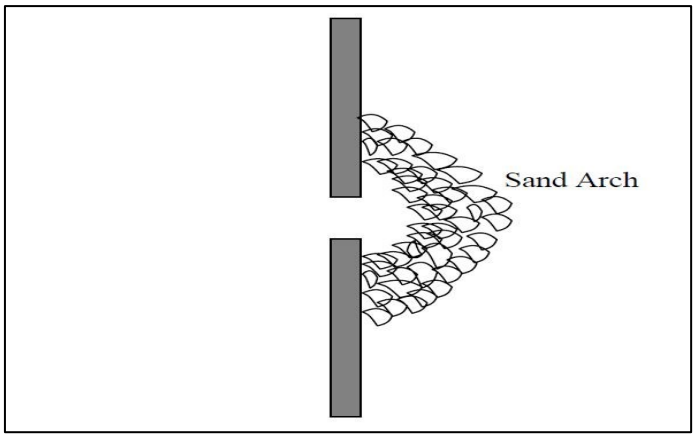

Figure 3: Sand Arch near Perforation [5]

They conducted several triaxial tests on unconsolidated sand samples to investigate the effects of fluid flow, sand roundness and wettability on the formation and the stability of the sand arch. It was observed that angular sands are more likely to form sand arch than round sands. It was also concluded that water cut tends to destroy the sand arch. More detailed experimental studies on the sand arch stability were conducted by Tippie and Kohlhaas (1973). They observed a growth in arch size with an increase in flow rate. As the size of the arch grows, it becomes less stable until it fails. After failure, new arches may form again, but they are usually larger and tend to fail at a lower flow velocity as compared to the previous arch. Cleary & al (1979) [6] observed that confining stress is also an important factor in the size and stability of sand arches. They reported that the arch size decreases with increasing confining stress. They also found that a more stable arch occurs when the horizontal stress is the maximum principal stress and the vertical stress is the minimum principal stress.

Bratli and Risnes (1981) [7] developed a theoretical model supported by laboratory studies to analyze the effect of stresses imposed by fluid flowing in sand arches and established a criterion for their stability. To obtain the analytical model, the geometry of the arch was simplified to a hemispherical shell of a porous media, figure 4.

The material is assumed to behave elastically until it fails according to a Coulomb failure criterion. Consequently, the shell will consist of an inner zone where the material has failed (Coulomb zone) and an outer zone where it still follows an elastic behaviour. The suggested stability criterion according to their model is

$$\frac{\mu q}{4\pi k r_1} = \frac{T+1}{T} 4 S_{co} \tan \alpha \tag{2.8}$$

Where q is flow rate, μ is the fluid viscosity, k is the permeability, r_1 is the radius of the inner surface, S_{co} is the cohesive strength, α is the failure angle, and T is a constant that depends on the failure angle such that:

$$T = 2(\tan^2 \alpha - 1) \tag{2.9}$$

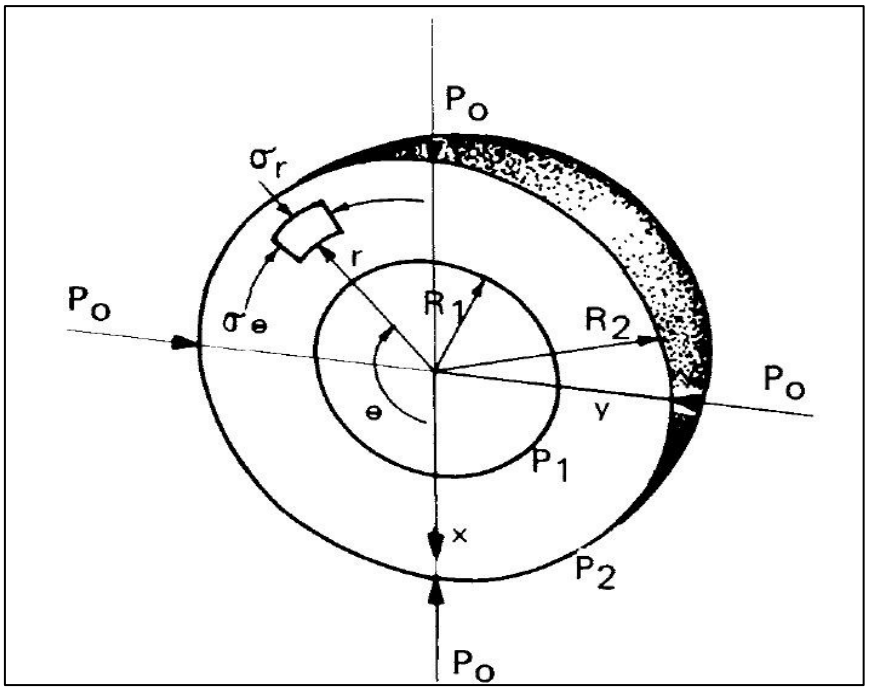

Figure 4: Theoretical Model: Hemispherical Shell [7]

According to this criterion, if the left-hand term exceeds the right-hand term, Eq-2.8, the Coulomb zone will extend through the entire system causing a total collapse of the sand arch.

Sand production can also be predicted by evaluating the well logs. Stein and Hilchie (1972) [8] proposed to estimate the formation strength by calculating the sand elastic properties from the velocities of acoustic shear and compressional waves obtained from sonic logs. It was concluded that the critical drawdown for the onset of sand production,Δp_c would be proportionately greater for stronger formation. They suggested the rock shear modulus, E_s as a parameter to represent the formation strength:

$$\Delta p_c \propto E_s \tag{2.10}$$

So, if the critical drawdown is known for a test zone, A, it is possible to estimate the critical drawdown in another interest zone, B, within the same formation by knowing the dynamic shear modulus through the equation:

$$(\Delta p_c)_B = (\Delta p_c)_A \frac{(E_s)_A}{(E_s)_B} \tag{2.11}$$

Tixier et al. (1975) [9] suggested a comprehensive method to estimate the sand production based upon the formation strength and elastic constants obtained from mechanical property logs, namely sonic and density logs. Through an experimental testing program, it was observed in their experiments that if the ratio of shear modulus to bulk compressibility, $^{G}/_{c_b}$ is above $0.8 \times 10^{12} psi^2$ it results in sand free product.

2.2.2 Failure Criteria

The most common mechanisms responsible for sand production are tensile failure, pore collapse and shear failure. The tensile failure may occur when the effective radial stress is equal to the tensile strength of the formation rock. The pore collapse is related to the depletion of the reservoir pressure. As the reservoir pressure decreases, the effective stress acting on the formation rock increases which will cause the collapse of the pores at a certain stress level. The shear failure is mainly related to the rock strength criterion. Different rock strength criteria are used to predict the onset of the sand production such as Mohr-Coulomb, Mogi-Coulomb, Drucker-Prager, and Modified Lade.

2.2.2.1 Mohr-Coulomb Criterion

The Mohr-Coulomb failure criterion [10] is one of the most widely used failure criterion in wellbore stability and sand production. It can be expressed by the following equation:

$$\tau = S_0 + \sigma \, tan \, \emptyset_f \tag{2.12}$$

Where

τ Shear stress [psi]

σ Normal stress [psi]

S_0 cohesive strength [psi]

ϕ_f internal friction angle [deg]

The Mohr-Coulomb criterion uses unconfined compressive strength (UCS) and the internal friction angle (ϕ_f) to assess the failure, and it is expressed in terms of principal stresses:

$$\sigma_1 = c_0 + \sigma_3 \frac{1 + \sin \emptyset_f}{1 - \sin \emptyset_f} \tag{2.13}$$

Where

σ_1 maximum principal stress [psi]

σ_3 minimum principal stresses [psi]

C_0 unconfined compressive strength [psi]

Based on the previous equation the failure function (F) can be written as follow:

$$F = c_0 + \sigma_3 \frac{1 + \sin \emptyset_f}{1 - \sin \emptyset_f} - \sigma_1 \tag{2.14}$$

Considering the Mohr-Coulomb failure criterion, shear failure occurs if $F \leq 0$.

Figure 5 shows the Mohr circle and Mohr-Coulomb strength envelope. The failure will occur if the values of σ_1 and σ_3 lie above the strength envelope. In the Mohr-Coulomb criterion, the main conclusion that should be taken into consideration is that the intermediate principal stress σ_2 does not affect failure and this may overestimate failure.

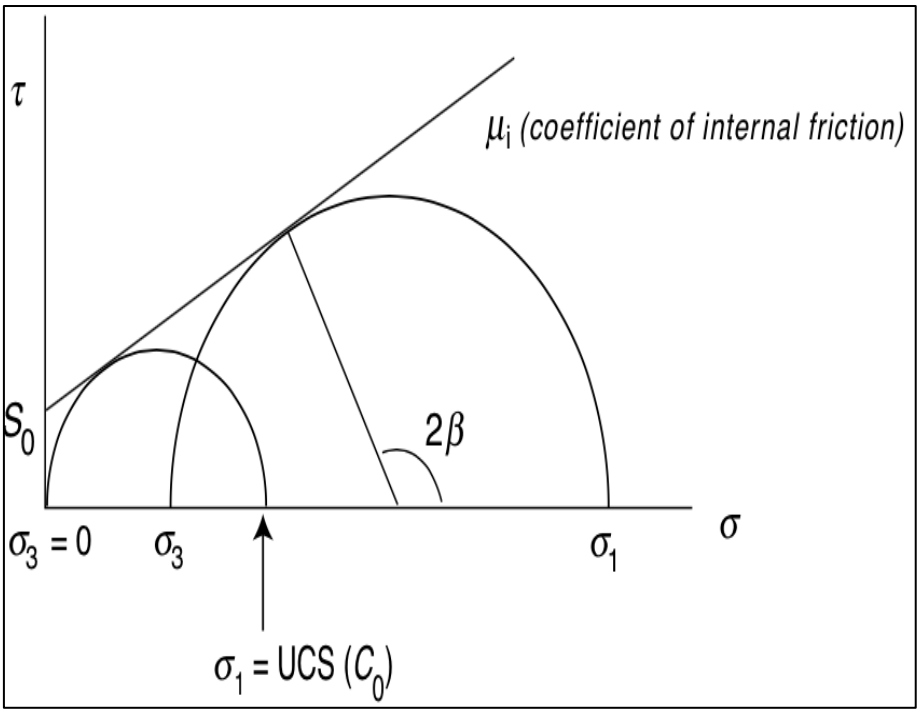

Figure 5: Mohr-Coulomb Failure Criterion [3, p. 88]

2.2.2.2 Drucker-Prager Criterion

Drucker-Prager [10] proposed their failure criterion as an extension to the Mohr-Coulomb criterion. In fact, they have considered the effect of the intermediate principle in the failure of the rock which has been neglected by the Mohr-Coulomb failure criterion.

The Drucker-Prager criterion can be expressed as follow:

$$\sqrt{J_2} = \alpha I_1 + k \tag{2.15}$$

Where:

$$I_1 = \sigma_1 + \sigma_2 + \sigma_3 \tag{2.16}$$

$$J_2 = \frac{1}{6}[(\sigma_1 - \sigma_2)^2 + (\sigma_2 - \sigma_3)^2 + (\sigma_1 - \sigma_3)^2] \tag{2.17}$$

I_1 First invariant of stress tensor

J_2 Second invariant of stress tensor

σ_2 Intermediate principal stress [psi]

α Constant

k Constant

The values of the two constants (k and α) in the Drucker-Prager criterion can be expressed in terms of the Mohr-Coulomb parameters S_0 and ϕ_f by matching two particular points with those of the Mohr-Coulomb criterion. Figure 6 shows that it is possible in various ways to relate the two failure criteria. In the case where the circumscribed Drucker-Parger envelope (compression), see figure 6, coincides with the other three apexes of the Mohr-Coulomb hexagonal pyramid, the two constants (k and α) in the Drucker-Prager criterion can be written as follows:

$$k = \frac{6S_0 \cos \emptyset_f}{\sqrt{3}(3 - \sin \emptyset_f)} \tag{2.18}$$

$$\alpha = \frac{2 \sin \emptyset_f}{\sqrt{3}(3 - \sin \emptyset_f)} \tag{2.19}$$

When the inscribed Drucker-Parger envelope (figure 6) coincides with the other three apexes of the pyramid, the constant has the following expressions:

$$k = \frac{6S_0 \cos \emptyset_f}{\sqrt{3}(3 + \sin \emptyset_f} \tag{2.20}$$

$$\alpha = \frac{2 \sin \emptyset_f}{\sqrt{3}(3 + \sin \emptyset_f)} \tag{2.21}$$

If the circumscribed Drucker-Parger envelope (extension) inscribes the Mohr-Coulomb hexagonal pyramid, the equations are:

$$\alpha = \frac{\tan \emptyset_f}{\sqrt{9 + 12 \tan {\emptyset_f}^2}} \tag{2.22}$$

$$k = \frac{3S_0}{\sqrt{9 + 12 \tan {\emptyset_f}^2}} \tag{2.23}$$

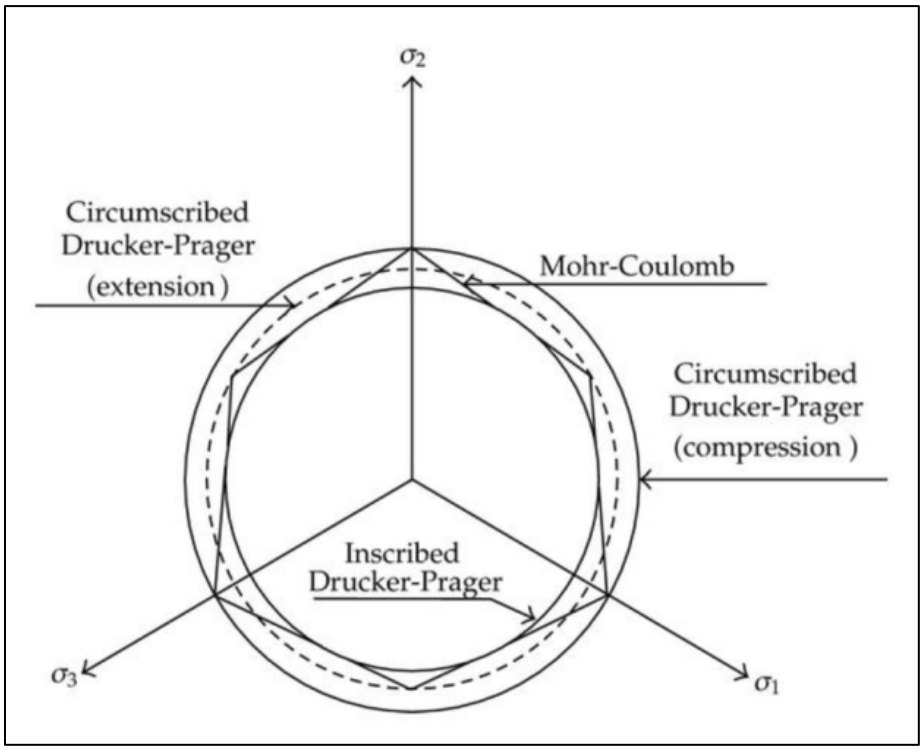

Figure 6: Failure Surfaces of Mohr-Coulomb and Drucker-Prager Criterion [11, p. 4]

2.2.2.3 Hoek-Brown Criterion

Hoek and Brown, 1980, proposed a rock strength criterion for the failure of the fractured rock. Therefore, this strength criterion included both rock and fracture properties:

$$\sigma_1 = \sigma_3 + \sqrt{c_0 s_h + m_h \sigma_3} \tag{2.24}$$

The two constants, s_h and m_h depend on the properties of the rock and on the extent to which it has been broken before being subjected to the stresses: s_h =1 for intact rock, s_h <1 for previously broken rock and m_h ranges from 0.001 (extremely week rock) to 25 (extremely strong rock).

Based on the previous equation the failure function (F) can be written as follow:

$$F = \sigma_3 - \sigma_1 + \sqrt{c_0 s_h + m_h \sigma_3} \tag{2.25}$$

According the Hoek-Brown criterion, shear failure occurs if $F \leq 0$.

Similar to the Mohr-Coulomb criterion, the Hoek-Brown failure criterion neglected the effect of the intermediate principal stresses. It is dependent on the maximum and the minimum principal stresses. The Hoek-Brown failure criterion, figure 7, is non-linear in contrast to the Mohr-coulomb criterion.

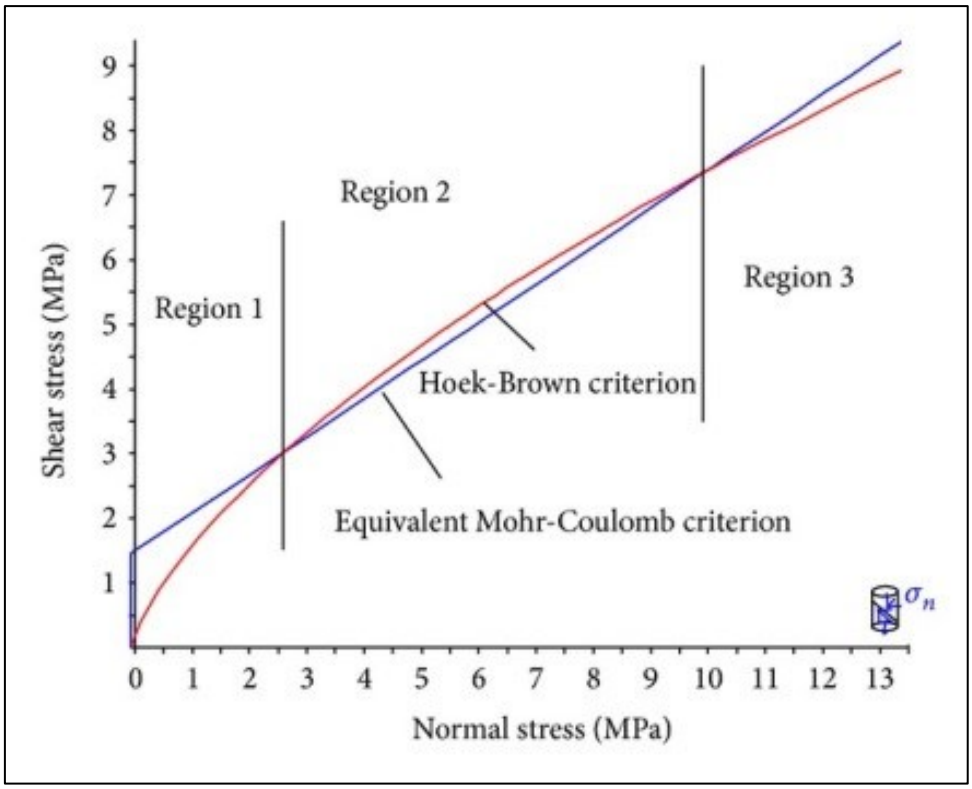

Figure 7: Hoek-Brown Failure Criterion [12, p. 5]

2.2.2.4 Modified-Lade Criterion

Ewy, 1998, proposed the modified Lade criterion based on the Lade, 1984, strength criterion. This modified strength criterion is dependent on the three principal stresses. Thus, the effect of the intermediate principal stress is considered in contrast to the precious criterion. The modified Lade criteria can be expressed by the following equation:

$$\frac{I_1^{"3}}{I_3^{"}} = 27 + \eta_L \tag{2.26}$$

Where:

$$I_1^{"} = (\sigma_1 + S_L) + (\sigma_2 + S_L) + (\sigma_3 + S_L) \tag{2.27}$$

$$I_1^{"} = (\sigma_1 + S_L)(\sigma_2 + S_L)(\sigma_3 + S_L) \tag{2.28}$$

The parameters S_L and η_L are material constants which can be expressed in terms of the cohesion of the rock, S_0, and the angle of the internal friction ϕ_F.

$$S_L = \frac{S_0}{\tan \phi_f} \tag{2.29}$$

$$\eta_L = \frac{4\tan^2\phi_f\,(9 - 7\sin\phi_f)}{1 - \sin\phi_f} \tag{2.30}$$

The failure function is

$$F = 27 + \eta_L - \frac{I_1^{"3}}{I_3^{"}} \tag{2.31}$$

Considering the Modified-Lade failure criterion, shear failure occurs if $F \leq 0$.

3 Geomechanical Properties from Well Logging Data

To implement the sand prediction model, the mechanical properties of the reservoir and overburden formation (rock strength, elastic properties, the state of in-situ stress and pore pressure) are calculated from the well log data. The calculated properties can be quickly evaluated and utilized with the model to predict sanding problem.

In this section, the detailed workflow, figure 8, for calculating and calibrating the different mechanical properties from the log data of this gas field is explained. Excel spreadsheet with user-friendly interface was developed to calculate the dynamic mechanical properties. (Appendix A)

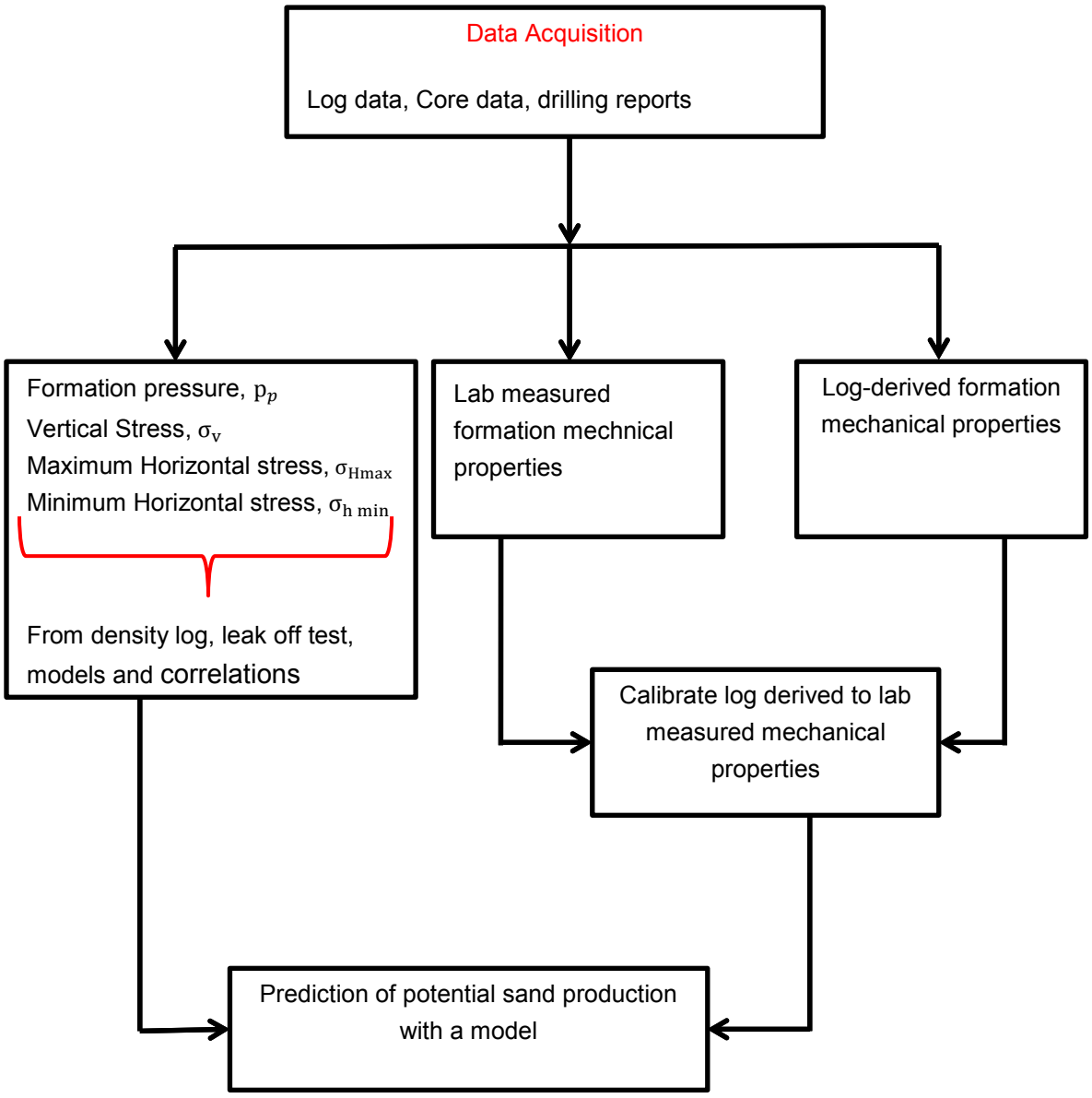

Figure 8: Procedure to Generate and Calibrate Mechanical Properties

3.1 Data Acquisition

The key data used to generate the geomechanical properties are micro-resistivity images, dipole sonic logs, formation pressure measurement, drilling reports, core data, density and Gamma-ray logs.

A data base of the drilling incidents including mud losses, caliper logs, OBMI images and stability incidents was compiled from the end of well reports for this gas field. This data base was later used to constrain and validate the stress model in section 3.4.4.

3.2 Dynamic Elastic Properties

There are several geomechanical properties used to describe the behaviour of a formation. The most common ones include Young's Modulus, Poisson's Ratio, Bulk Modulus, and Shear Modulus.

Two approaches are used for determining the elastic moduli. One method consists of generating the elastic constants from the stress-strain relationship, hence called the 'static elastic constants'. The other method is based upon measurements of elastic wave velocities to determine the elastic moduli which are called the 'dynamic elastic constants'. The solution derived in this study is static and, therefore, the dynamic properties must be corrected by using dynamic-static properties correlations for the investigated rock.

In this model, two methods have been adopted for determining the dynamic measurement from the well log data. First, if the sonic shear log data was available, then the dynamic elastic moduli are determined from the transit time of compressional and shear waves using the following relationships:

$$E_{dyn} = \frac{\rho_b(3{\Delta t_S}^2 - 4{\Delta t_C}^2)}{1 - (\frac{\Delta t_C}{\Delta t_S})^2} * 1.34 * 10^{10} \tag{3.1}$$

$$\mu_{dyn} = \frac{0.5(\Delta t_S/\Delta t_C)^2 - 1}{(\frac{\Delta t_S}{\Delta t_C})^2 - 1} \tag{3.2}$$

$$G_{dyn} = \frac{\rho_b}{\Delta t_S^2} * 1.34 * 10^{10} \tag{3.3}$$

$$K_{dyn} = \rho_b \left[{}^{1}/_{\Delta t_C^2} - {}^{4}/_{3\Delta t_S^2} \right] * 1.34 * 10^{10} \tag{3.4}$$

ρ_b Bulk density gm/cc

Δt_C Compressional transit time us/ft

Δt_C Shear transit time

$1.34 * 10^{10}$ Factor to convert bulk and shear moduli in psi unit

Second, in the absence of shear sonic data which was the case in this studied field, an alternative approach is adopted for calculating elastic properties using only compressional sonic data. This approach is based on the empirical relationship which related shaliness index to the Poisson's ratio of the sand as described by Anderson et.al [13].

In this study, the empirical relationship between Poisson's ratio and shaliness has been generated from log data of an offset well from the field region where both shear and compressional logs are recorded.

Based upon the plot of the Poisson´s ratio versus shaliness index (I_{sh}) as shown in figure 9, the following linear relationship was obtained:

$$\mu_{dyn} = 0.167 * I_{sh} + 0.187 \quad (3.5)$$

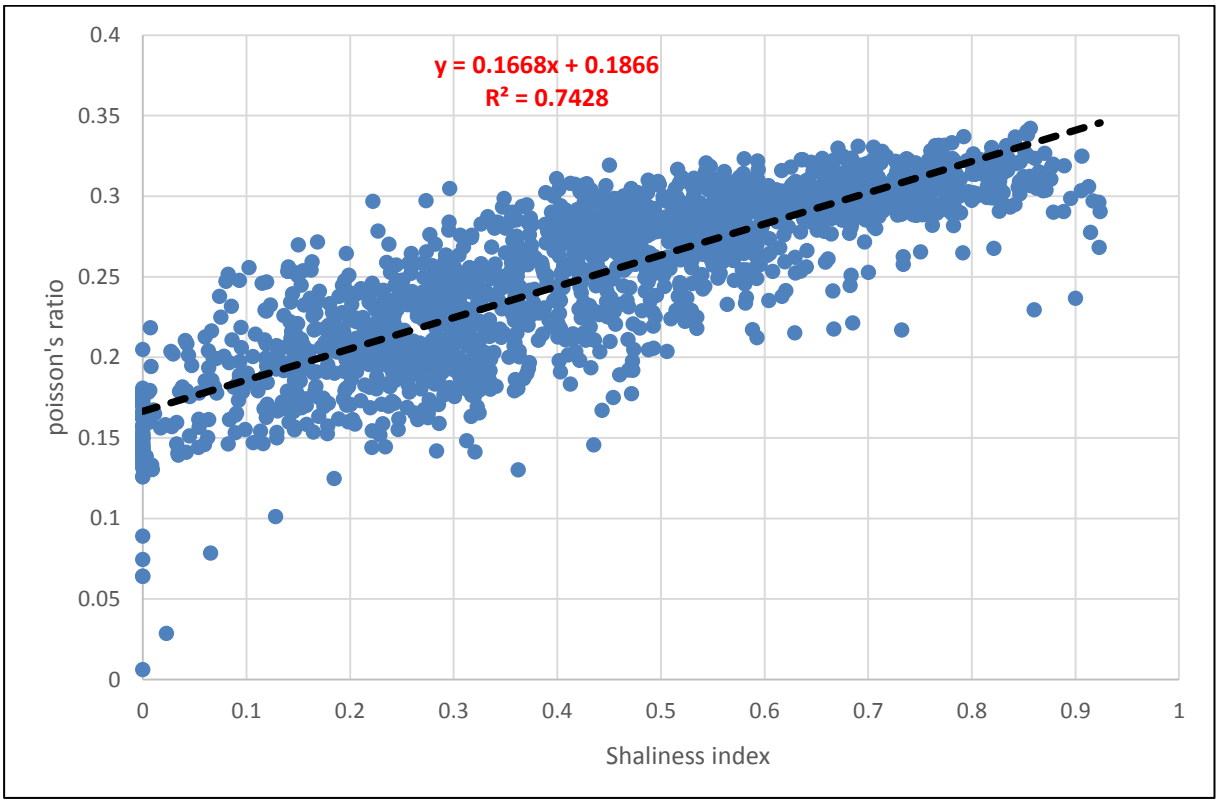

Figure 9: Empirical Relationship between Poisson's Ratio and Shaliness Index

Once the empirical relationship between the Poisson's and the shaliness index has been established, then the dynamic Poisson's ratio for each well is calculated as a function of the shaliness index data according to Eq.3.5

The other dynamic elastic moduli (Young's Modulus, Bulk Modulus, and Shear Modulus) are computed as a function of the compressional transit time and the dynamic Poisson´s ratio generated from the shaliness index data in the following way:

$$E_{dyn} = \frac{(1-2\mu_{dyn})(1+\mu_{dyn})}{(1-\mu_{dyn})}\left(\rho_b/\Delta t_C^2\right) * 1.34 * 10^{10} \quad (3.6)$$

$$G_{dyn} = \frac{1-2\mu_{dyn}}{2(1-\mu_{dyn})}\left(\rho_b/\Delta t_C^2\right) * 1.34 * 10^{10} \quad (3.7)$$

$$K_{dyn} = \frac{1+\mu_{dyn}}{3(1-\mu_{dyn})}\left(\rho_b/\Delta t_C^2\right) * 1.34 * 10^{10} \quad (3.8)$$

Several relationships between static and dynamic Young's modulus for different types of rocks were developed by various authors [14]. Vanheerden (1987) proposed the following relationship for sandstone rocks:

$$E_{sta} = a * {E_{dyn}}^b \quad (3.9)$$

Where the two rock parameters (a, b) are determined from the laboratory testing.

The previous correction function, Eq 3.9, is used to generate the static Young's modulus for the reservoir rocks in this study field. The two parameters (a, b) are calculated based on laboratory testing of core samples taken from Well-1 in this gas field. As a result, the following correction is obtained:

$$E_{sta} = 0.095 * {E_{dyn}}^{1.48} \quad (3.10)$$

Figure 10 shows the dynamic and static elastic properties for Well-1.

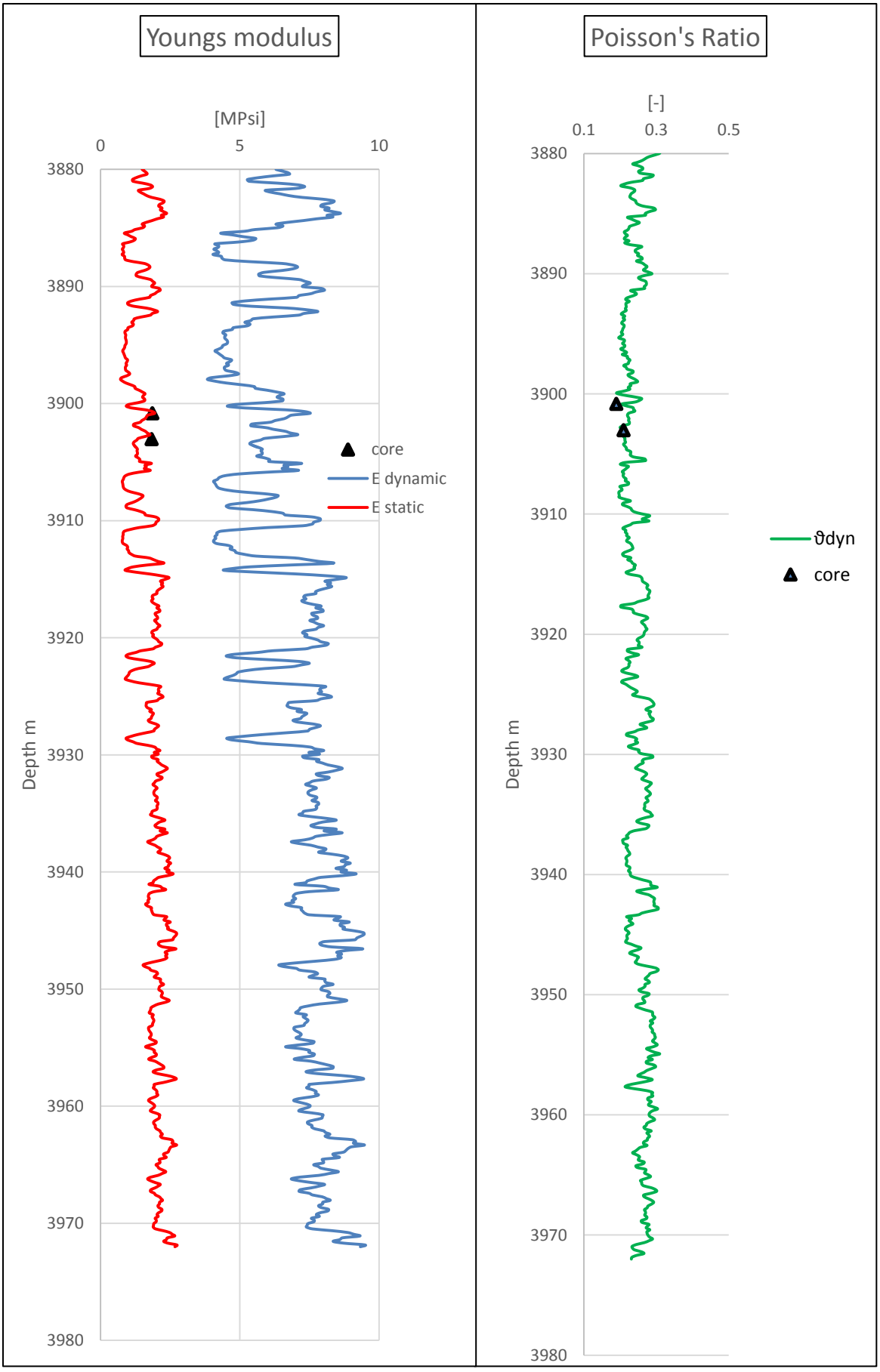

Figure 10: Elastic Properties Profiles for Well-1

3.3 Rock Strength

The widely used rock strength parameters for geomechanical analysis are the uniaxial compressive strength (UCS) and thick wall cylinder strength (TWC). The rock strength parameters can be generated from the well log data using several log strength correlations. The developed sand prediction model requires the TWC strength to estimate the strength of the formation (see section 4.4.2) and the UCS values to estimate the maximum horizontal stress. (See section 3.4.4)

In this section, the procedure of calculating and calibrating the rock strength properties from the log data of this gas field is explained.

3.3.1 Core Strength Data

Rock strength measurements made in the laboratory are used to calibrate the open-hole log derived continuous formation strength model.

The Uniaxial core test is an unconfined test in which a force is an applied parallel to the axis of the core sample. No lateral forces are applied and therefore it is also called unconfined compressive test. The unconfined compressive strength reflects the amount of the stress a rock can withstand without failing [15].

The triaxial core test, figure 11, is a confined test that measures strength at different levels of confining pressure. Axial and confining pressures are applied to the core sample. The lateral force is increased until the desired confining pressure is reached then it is held constant [15]. The magnitude of the axial stress is increased until the sample failure is reached. The stress at failure is the confined compressive strength. The two Mohr-Coulomb parameters, the cohesion and the angle of internal friction are determined from multiple confined core tests.

The hole-collapse strength (HCS) test, called also a thick hollow cylinder test (TWC), is conducted to simulate the perforation tunnel failure. The standard dimensions for the HCS samples are the 1.5-inch diameter and approximately 2-inch length. Before the test, a 0.5-inch diameter hole is drilled axially through the center of the core sample. The geometry and loading of a hole-collapse specimen are illustrated in figure 12.

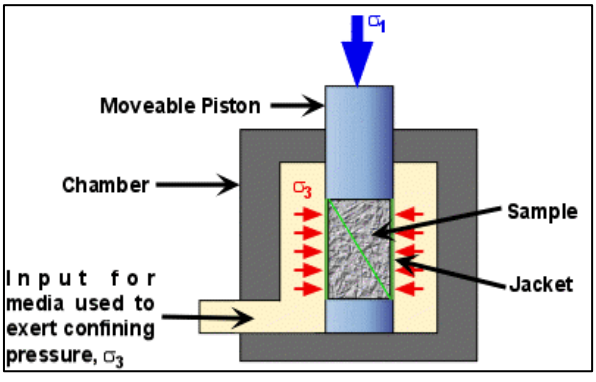

Figure 11: Triaxial Collapse Test

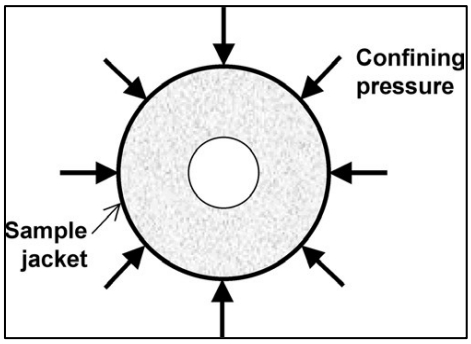

Figure 12: Geometry and Loading of a Hole-Collapse Sample [16, p. 244]

In this study, the rock strength measurements made in the laboratory are used to calibrate the rock strength parameters calculated from the well log data (section 3.3.2). Testing included unconfined compressive strength (UCS) and thick-walled cylinder (TWC) tests. The results of the rock mechanical test conducted on the core samples from this field are shown in Appendix-C

3.3.2 Log Strength Model

The unconfined compressive strength (UCS) and the thick wall cylinder strength (TWC) of sedimentary rocks are important parameters to assess sanding potential and wellbore instability. The Uniaxial core test is used to generate the values of UCS and TWS from the core samples obtained from the depth of interest. However, the laboratory tests cannot provide continuous measurement of the rock strength at the reservoir section. Therefore, a number of empirical correlations are used in the literature that relates the rock strength parameters to parameters measurable with petro-physical well logs which result in a continuous rock strength model [17]. The four most commonly used correlations for sandstone reservoirs described below are implemented in the sand prediction excel model (see Appendix-A).

Freyburg, 1972, developed a correlation between UCS and the compressional wave velocity based on the data in Thuringa, Germany [17]:

$$UCS = 0.35V_P - 31.5 \tag{3.11}$$

For fine-grained, both consolidated and unconsolidated sandstones in the Bowen Basin of Australia, McNally (1987) presented the following strength estimation using sonic logs [17]:

$$UCS = 1200e^{-0.036\Delta t_C} \tag{3.12}$$

For weak and unconsolidated sandstones in the U.S. Gulf Coast the following empirical equation exists [17]:

$$UCS = 1.4138 * 10^{10}\Delta t_C^{-3} \tag{3.13}$$

Vernick et al proposed two models: Vernick-1 and Vernick-2 which are respectively referred to as [17]:

$$UCS = 254(1 - 2.7\emptyset)^2 \quad (3.14)$$

$$UCS = 277e^{-10\emptyset} \quad (3.15)$$

Vernick-1 is applicable for very clean, well-consolidated sandstones with porosities less than 30%, whilst Vernick-2 is applicable to sandstones with UCS in the range from 300 psi to 50000 psi and porosities from 0.2% to 33%.

The majority of the generic UCS models over-predict the rock strength compared to the core results of the study field. The U.S Gulf Coast correlation gave the best fit but tends to over-predict the strength slightly. Therefore, the U.S Gulf Coast correlation is used to create a continuous UCS profile in the target sands for all study wells. The empirical core-log rock strength plots derived from logs of Well 1 are shown in figure 13.

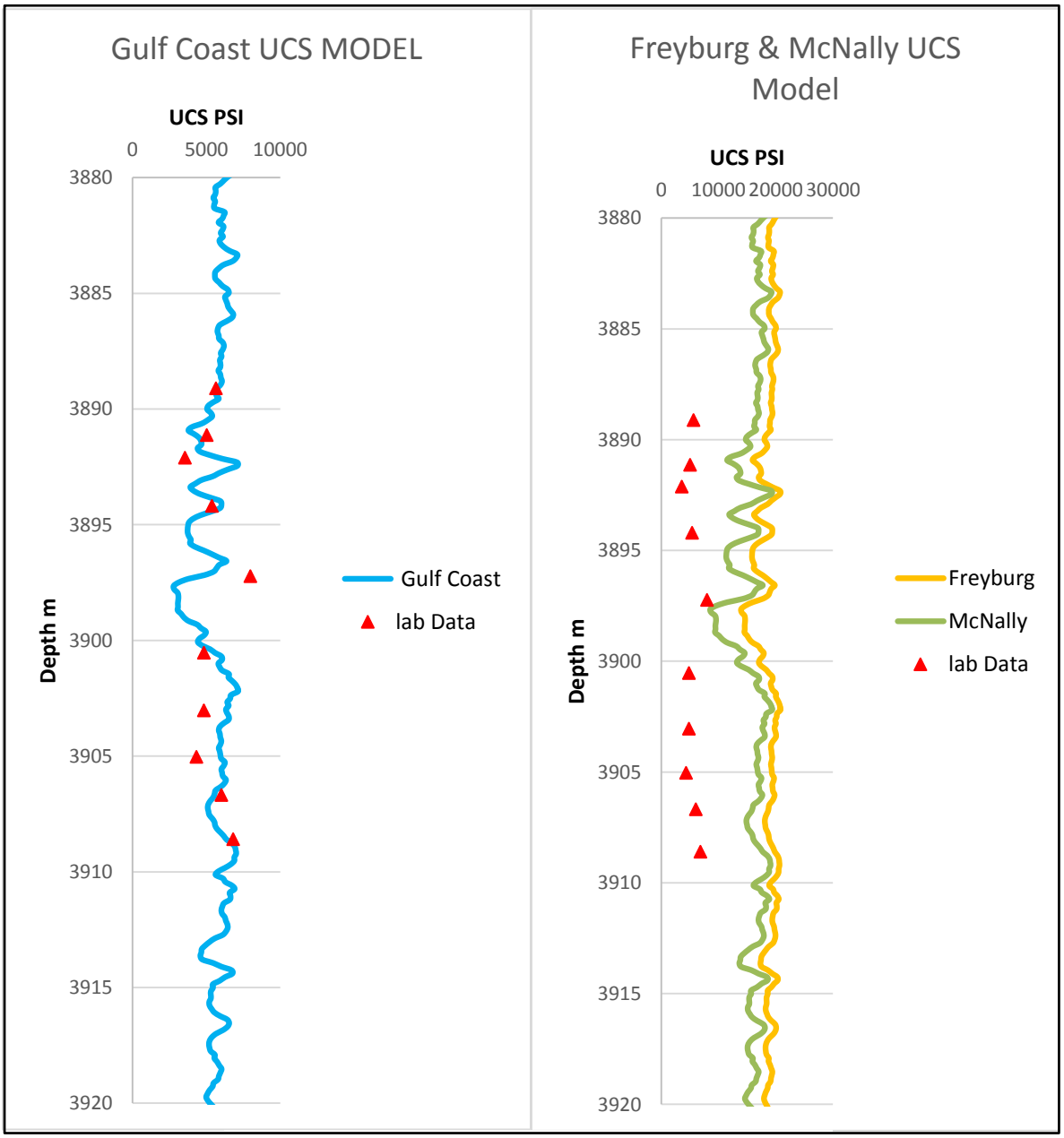

Figure 13: Empirical Core-Log UCS Plots for Well-1

Similar to the UCS, the dynamic TWC strength is calculated based on empirical relationship which is developed by Tronvoll [18]:

$$TWC = 37.59 * UCS^{0.6346} \tag{3.16}$$

This empirical equation is considered in the excel model to generate the TWC profile from well log data of the wells in the study field as it gives the best fit to the laboratory measurement. Figure 14 shows the TWC strength profile calculated from the well log data of Well-1.

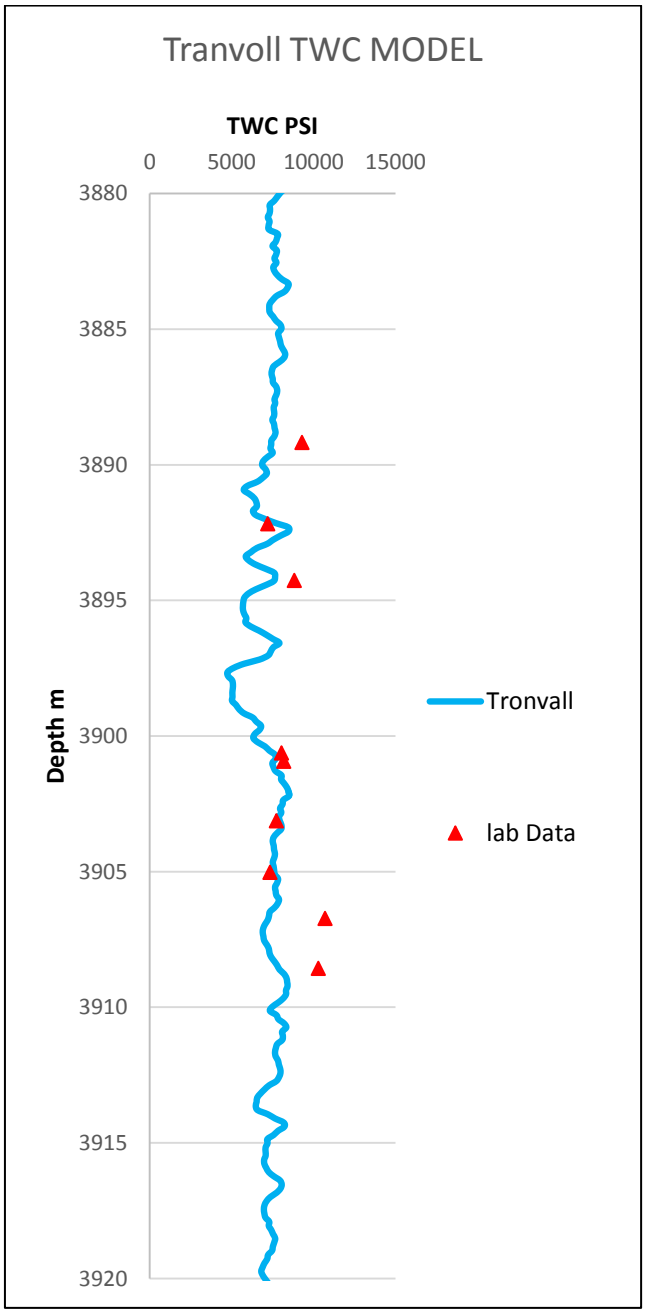

Figure 14: TWC Strength Profile of Well-1

As discussed above, the rock strength profile for the reservoir section was estimated from log modeling based on empirical correlations. Therefore, the statistical analysis of the distribution of log-derived strength (UCS and TWC) values were established for the study field due to uncertainty. The developed model can accommodate the three case sensitivities (P10 P50 and P90) for the sanding evaluation for each well (see Appendix-A). The percentiles (P10, P50, and P90) were determined from the distribution of the log-derived strength where P10 represents the weakest 10% of the rock in the interval and it is taken as the base case for the sanding evaluation (see section 4.4). Figure 15 shows the distribution of the log-derived UCS for Well-1. The three case sensitivities for the UCS strength of Well-1 is summarized in table1.

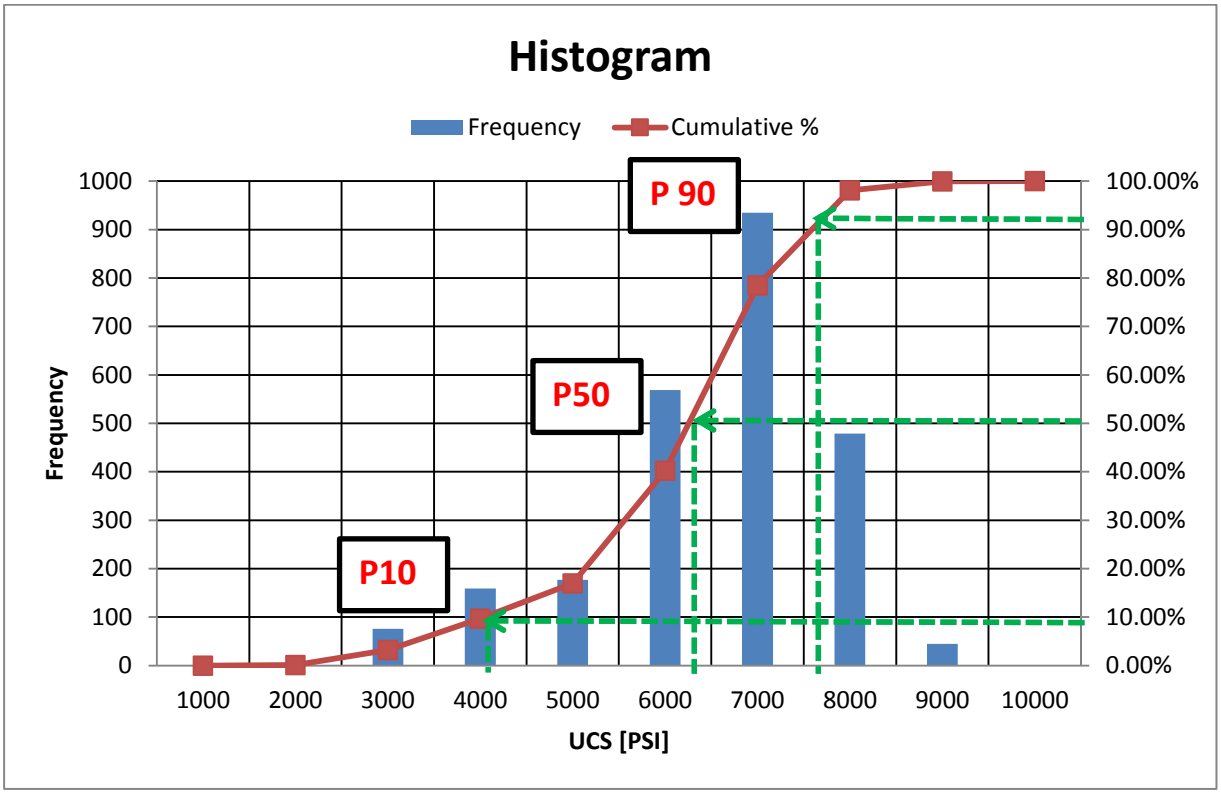

Figure 15: UCS Strength Distribution for Well-1

Table 1: UCS Percentiles Cases for Well-1

	UCS [PSI]
P10	4038
P50	6290
P90	7350

3.4 In-situ Stress Model

The in-situ stress model provides the stress distribution around the wellbore and/or the perforation cavity. The key input data used to build the wellbore stress model are the pore pressure and the far-field reservoir stresses: vertical stress, maximum and minimum horizontal stress.

3.4.1 Pore Pressure

There is a variety of methods available to determine the pore pressure. Such methods include drilling, logging, and seismic data. For this study, MDT data was available for all wells to evaluate pore pressure. Based on the MDT measurement, a pore pressure gradient of $0.47\,psi/ft$ was considered for the studied field.

3.4.2 Vertical Stress

The vertical stress is generally calculated through integrating the bulk density along true vertical depth as it is expressed in the following equation:

$$\sigma_v = \int_0^Z \rho_b(z)dz \tag{3.17}$$

Bulk density logs were available for all studied wells from 1700 m TVD to total depth. Missing density log at shallow depths was calculated by using the density measurement of two offset wells. A vertical stress gradient of $1.07\,psi/ft$ was calculated for the reservoir datum.

3.4.3 Minimum Horizontal Stress

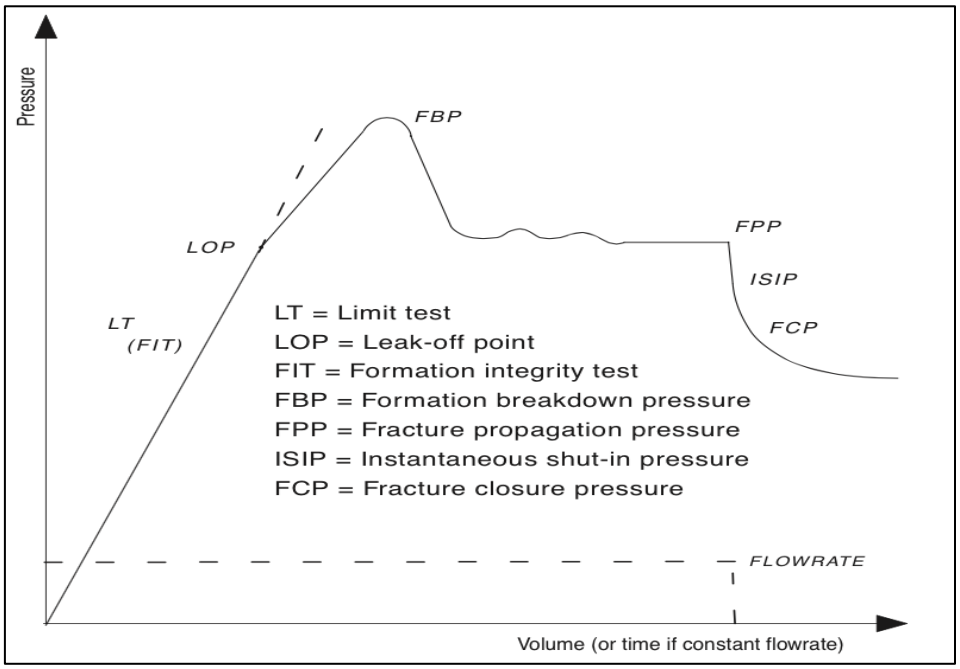

Figure 16: General Pressure vs Time/Volume Plot of a Hydraulic Fracture Test [3, p. 211]

The hydraulic fracture tests, Leak-off test (LOT) and Formation integrity test (FIT), can be used to determine the minimum horizontal stress. In a LOT, figure 16, only the hole below the casing and any new formation drilled prior to the test are exposed. Fluid is pumped into the hole with a constant flowrate. The pressure increase in the hole is monitored and pressure increase is typically linear as long as there are no breaks in the formation. The pressure is augmented until an increased leak-off to the formation due to fracture initiation is seen. The leak-off pressure (LOP) is indicated by the point of deviation from the linear pressure-time curve and corresponds to fracture initiation. The peak fracture breakdown pressure (FBP) is higher than the LOP and marks the onset of unstable fracture propagation [10] The FBP can be significantly higher than the LOP, depending on the tensile strength of the rock, and the presence of crack-blocking additives in the drilling fluid. If pumping is continued (e.g. in an XLOT) the pressure reduces to the stable fracture propagation pressure (FPP). After the well is shut in, the pressure begins to drop and the fracture starts to close. In the LOT test, the minimum horizontal stress is equal to the fracture closure pressure (FCP) [10]. The closure pressure can be determined from the “G-function” or the “Square Root Time”, Sqrt (t), plot. The G-function is a dimensionless time function relating shut-in time to total pumping time at an assumed constant rate and the closure pressure is identified as the point where the G-Function derivative starts to deviate downward from the straight line as shown in figure 17. Using the Sqrt (t) plot, the fracture pressure can be identified by the peak of the first derivative, which corresponds to an inflection point on the pressure curve as shown in figure 18. [19]

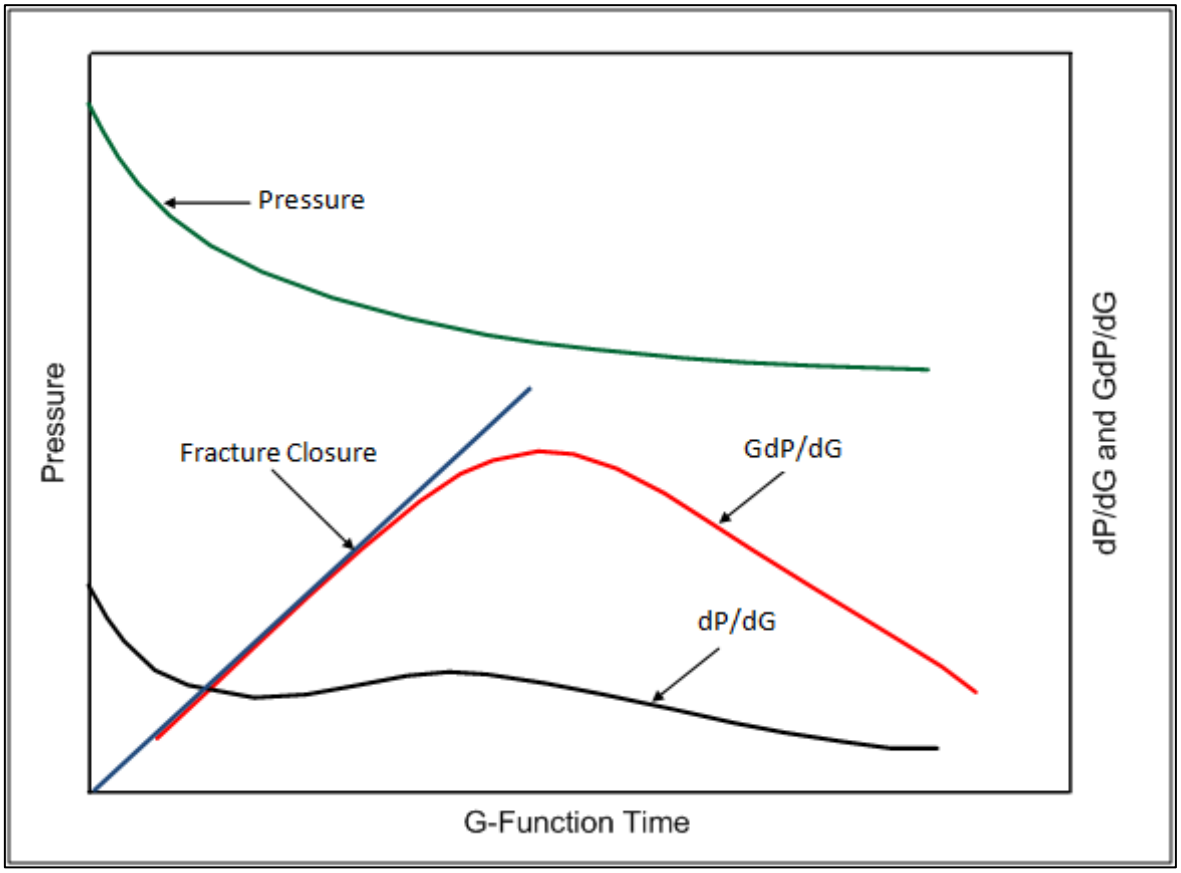

Figure 17: G-Function Plot [19]

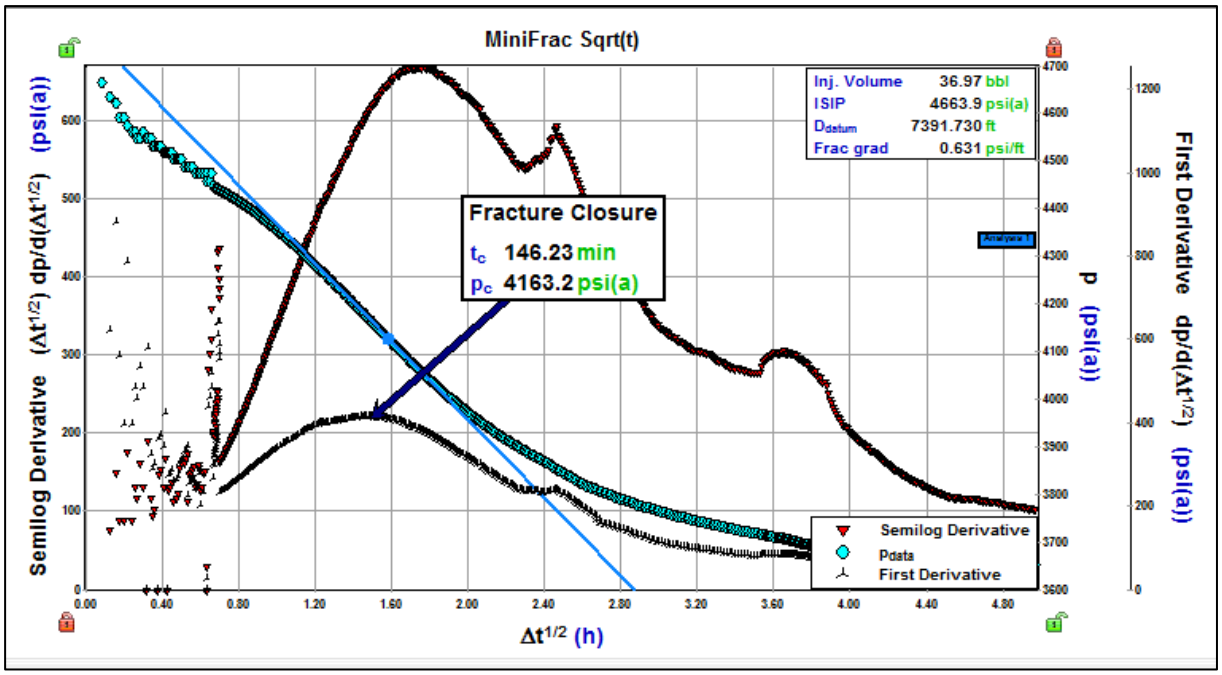

Figure 18: Square Root Time Plot [19]

In the FIT the well pressure is increased to some pre-set value, which has been selected based on an evaluation of what well pressures will be reached during safe drilling of the next borehole section. The main purpose of the FIT is to verify the quality of the cementing of the casing without breaking the formation. Therefore, the FIT test is used to estimate the lower limit for the minimum horizontal stress gradient.

If there is no LOT or FIT data available at the depth of interest, variety of empirical relations are available to determine the magnitude of the horizontal stresses. Such methods include elastic modeling theory and other correlations. Minimum horizontal stress is conventionally calculated using the following elastic model:

$$\sigma_{h\,min} = \frac{\vartheta}{1-\vartheta}\left(\sigma_v - \alpha p_p\right) + \alpha p_p \tag{3.18}$$

Where:

$\sigma_{h\,min}$	Minimum horizontal stress
σ_v	Vertical stress
ϑ	Poisson´s ratio
α	Biot´s poroelastic factor: $0 \leq \alpha \leq 1$
p_p	Pore pressure

It is based on the assumption of the bilateral constraint which is assumed that the only source of horizontal stress is the overburden and that the two horizontal stresses are equal in

magnitude. This uniaxial horizontal stress condition is only valid for a passive basin, no tectonic stress.

Breckels and Van Eekelen proposed a relationship between minimum horizontal stress and depth. These relationships were based on hydraulic fracture data from different regions around the world. In these relationships, the abnormal pore pressure effects were also considered [20]. It is expressed as follows:

$$\sigma_{h\,min} = 0.197Z^{1.145} + 0.46(p_p - p_{pn}) \qquad For\ Z < 11{,}500\ ft \tag{3.19}$$

$$\sigma_{h\,min} = 1.167Z - 4596 + 0.46(p_p - p_{pn}) \qquad For\ Z > 11{,}500\ ft \tag{1.20}$$

Where

p_{pn} Normal pore pressure corresponding to a gradient value of $0.465\ {}^{psi}/_{ft}$ [20]

P_p Pore pressure [psi]

Z Depth [ft]

It is argued that these relationships can be used with a fair degree of confidence also in other tectonically relaxed areas of the world for sandstone reservoirs. Thus, these relations may provide reasonable estimates, but should only be considered as a first estimate and should always be calibrated against proper test data from each field

In the present study, there is no FIT and LOT data available for the reservoir interval. Thus, two stress case sensitivities are selected as first estimations for the minimum horizontal stress gradient for the study field, table 2.

Table 2: Minimum Horizontal Stress Cases

	$\sigma_{h\,min}$ Gradient (psi/ft)	Correlation
Case1	0.66	Elastic model
Case2	0.78	Breckels and Van Eekelen

3.4.4 Maximum Horizontal Stress

Maximum horizontal stress determination is crucial as there are no methods available so far to measure directly the magnitude of the maximum horizontal stress. The commonly used method to estimate the magnitude of the maximum horizontal stress is through the back analysis of wellbore failures, such as drilling induced fractures and breakouts.

Therefore, the analysis of the rock strength conditions under which wellbore failure occurred together with vertical stress and minimum horizontal stress can help to compute the magnitude of the maximum horizontal stress. In fact, shear failure, such as breakout, occurs at the borehole wall when a low mud weight pressure creates a large enough stress differential between the maximum principal stress and the minimum principal stress to exceed the failure criterion for that layer. The collapse mud weight that causes shear failure can be used to estimate the maximum to minimum horizontal stress; $\sigma_{H\,max}/\sigma_{h\,min}$ ratio. The calculation approach of the maximum to minimum horizontal stress ratio is divided into the following stages. In the first stage, a rock strength failure is selected to calculate the collapse mud weight at different $\sigma_{H\,max}/\sigma_{h\,min}$ values. The predicted collapse mud weight was then compared with the previous drill history collected in the drilling knowledge database of the studied wells.

In the study field, there were Caliper logs and image logs showing borehole washouts and breakouts at the reservoir depth. By following the previous procedure, the Modified-Lade criterion (see section 2.2.2.4) is selected as the rock failure criterion to compute the collapse mud weight. Using the Modified-Lade criterion the critical wellbore pressure to prevent instability for a vertical wellbore, P_{wc} is given by [21]:

$$P_{wc} = \frac{(B - \sqrt{C})}{2A} \tag{3.21}$$

Where

$$A = \sigma_z + S_L - p_p \tag{3.22}$$

$$B = A\sigma_\theta \tag{3.23}$$

$$C = B^2 - 4A\{D - (S_L - p_p)[A(\sigma_\theta + S_L - p_p]\} \tag{3.24}$$

$$D = (\sigma_\theta + \sigma_z + 3S_L - 3p_p)/(27 + \eta_L) \tag{3.25}$$

$$\sigma_\theta = 3\sigma_{h\,min} - \sigma_{H\,max} \tag{3.26}$$

$$\sigma_z = \sigma_v - 2\vartheta(\sigma_{H\,max} - \sigma_{h\,min}) \tag{3.27}$$

The study of the sensitivity on the magnitude of the maximum horizontal stress was conducted for the two minimum horizontal stress cases at the reservoir depth (approximately 3900 m). The Vertical stress and the pore pressure were the same for all the cases. As

discussed in section 3.2.2, the UCS strength for the reservoir section was determined by computing the percentiles from the standards distribution of the log derived UCS strength. The P10 was taken as the base case to constrain the magnitude of the maximum horizontal stress. The tables 7, 8, and 9 summarise the input data and the collapse mud weight (CMW) prediction for all the cases.

Table 3: Input Data and Predicted Mud Weight for $S_{hmin} = S_{hmax}$

	Depth (m)	S_v (psi)	Pp (psi)	S_{hmin} (psi)	S_{hmax} (psi)	P10 UCS (psi)	CMW (ppg)	Drill History (ppg)
Case1	3900	13706	6014	8445	8445	4050	9.02	9.7-10.3
Case2	3900	13706	6014	9991	9991	4050	9.25	9.7-10.3

Table 4: Input Data and Predicted Mud Weight for $Sh_{max} = 1.2\ S_{hmin}$

	Depth (m)	S_v (psi)	Pp (psi)	S_{hmin} (psi)	S_{hmax} (psi)	P10 UCS (psi)	CMW (ppg)	Drill History (ppg)
Case1	3900	13706	6014	8445	10134	4050	9.4	9.7-10.3
Case2	3900	13706	6014	9991	11989	4050	9.97	9.7-10.3

Table 5: Input Data and Predicted Mud Weight for $Sh_{max} > S_v$

	Depth (m)	S_v (psi)	Pp (psi)	S_{hmin} (psi)	S_{hmax} (psi)	P10 UCS (psi)	CMW (ppg)	Drill History (ppg)
Case1	3900	13706	6014	8445	14356	4050	12.15	9.7-10.3
Case2	3900	13706	6014	9991	16985	4050	14.61	9.7-10.3

According to the caliper logs, all wells (9.7 - 10.3 ppg) had minor hole enlargement. The Oil Base Micro-Imager image (OBMI) of the well 1 shows a borehole breakout at the reservoir section [1]. For all stress cases if $S_{hmax} > S_v$, the wells could not have been drilled successfully with the mud weights previously used. As a result, the study field is associated with a normal-faulting stress regime, $S_{hmin} < S_{hmax} < S_v$.

The calculated collapse mud weight for stress case 2 with $\frac{\sigma_{H\,max}}{\sigma_{h\,min}}$ range from 1.15 to 1.2 (see table 4) was in agreement with drilling experiences and the wellbore failures inferred from the image-log and caliper data of the drilled wells. Therefore, the case 2 for the minimum horizontal stress with $1.15 \leq \frac{\sigma_{H\,max}}{\sigma_{h\,min}} \leq 1.2$ was selected as the first estimate for the horizontal stresses gradients in this gas field.

3.4.5 Stress Orientation

The orientation of the stress field is essential information in the evaluation of the wellbore stability and the sand production. There is a variety of methods available to determine the orientation of the stress field. Such methods include breakouts and drilling-induced fracture interpretation from borehole image logs and caliper data analysis [22]. In a vertical well, the maximum tangential stress that results in Breakouts at the wall of the borehole is in a direction parallel to the minimum horizontal stress (Figure 19).

For this gas field, The OBMI image data and interpretation reports were available for all study wells [1]. The breakout has a dominant NE-SW direction. Consequently, the in situ S_{hmin} strikes NE-SW and the in situ S_{hmax} is therefore expected to be perpendicular to this, which means in the direction of NW-SE.

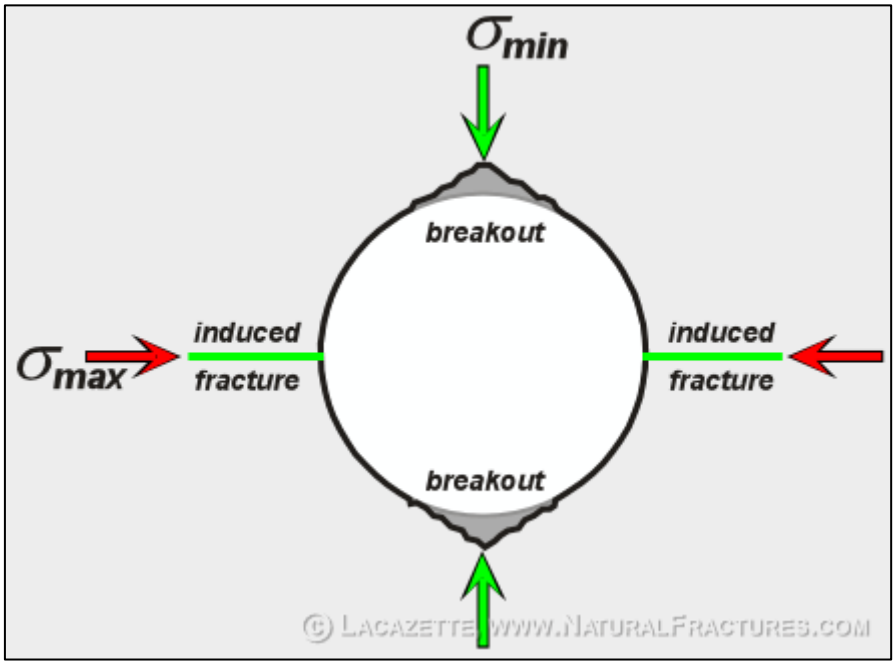

Figure 19: Breakout in Vertical Wells

4 Sand Prediction Model

This section discusses the methods for calculating the stress distribution around the wellbore for open-hole completion or the perforation for cased-hole completion and for applying proper failure criteria for sanding evaluation.

4.1 Stress Distribution around the Wellbore

The coordinate system (X', Y', Z') is defined by the three principal in-situ stresses as shown in Figure 20. In this coordinate system, the overburden stress, σ_v, is parallel to the Z'-axis, the maximum horizontal stress, σ_{hmin}, is parallel the X'-axis, and the minimum horizontal stress, σ_{Hmax}, is parallel to the Y'-axis.

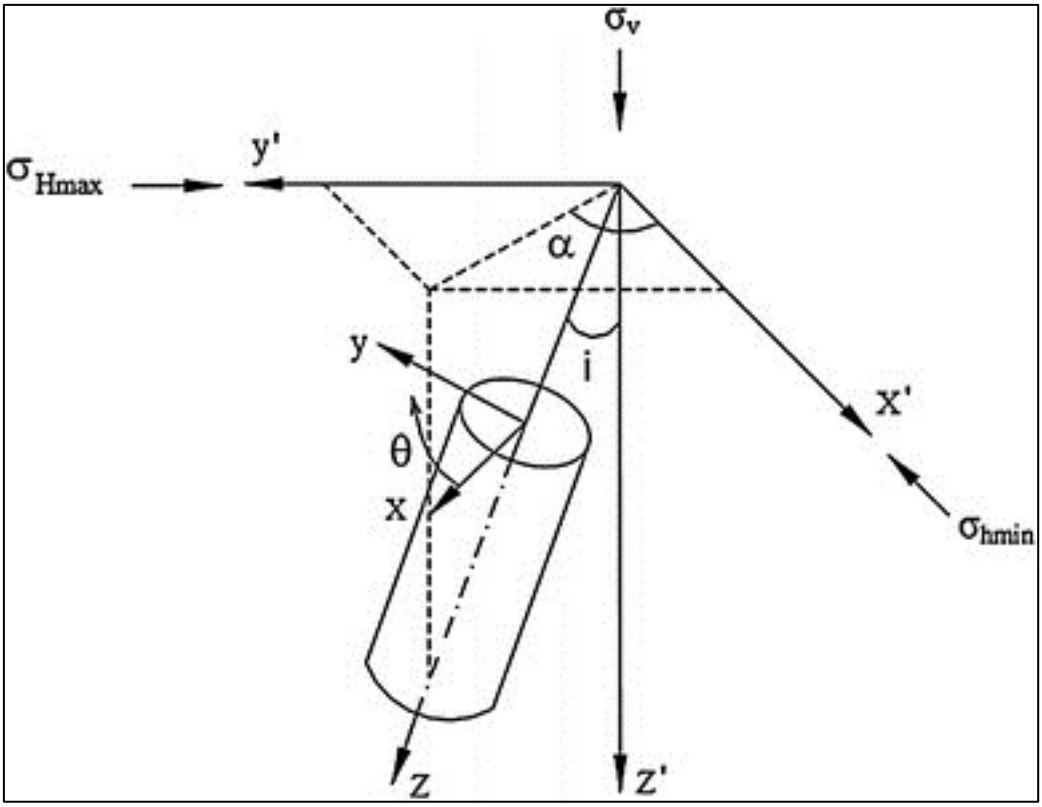

Figure 20: Stress Transformation System for a Deviated Wellbore

The in-situ stresses in the Cartesian coordinate system (x, y, and z) referred to the borehole are given by:

$$\sigma_x = (\sigma_{H\,max}\cos^2\alpha + \sigma_{h\,min}\sin^2\alpha)\cos^2 i + \sigma_v \sin^2 i \tag{4.1}$$

$$\sigma_y = (\sigma_{H\,max}\sin^2\alpha + \sigma_{h\,min}\cos^2\alpha) \tag{4.2}$$

$$\sigma_z = (\sigma_{H\,max}\cos^2\alpha + \sigma_{h\,min}\sin^2\alpha)\sin^2 i + \sigma_v \cos^2 i \tag{4.3}$$

$$\sigma_{xy} = 0.5(\sigma_{h\,min} - \sigma_{H\,max})\sin 2\alpha \cos i \tag{4.4}$$

$$\sigma_{yz} = 0.5(\sigma_{h\,min} - \sigma_{H\,max}) \sin 2\alpha \sin i \tag{4.5}$$

$$\sigma_{xz} = 0.5(\sigma_{h\,min} \cos^2 \alpha - \sigma_{H\,max} \sin^2 \alpha - \sigma_v) \sin 2\alpha \sin i \tag{4.6}$$

The angle α is the angle between the hole inclination (projection on plane) and σ_{Hmax} direction and it is defined counter-clockwise positive from σ_{Hmax} direction. The angle i is the borehole inclination with respect to the vertical [23].

The polar coordinate system is generally adopted to analyze the stress and pore-pressure distribution around wellbores. The stresses in polar coordinates are related to the Cartesian-coordinate stresses according to the following rules [3]:

$$\sigma_{\theta\theta} = \sigma_x + \sigma_y - 2(\sigma_x - \sigma_y) \cos 2\theta - 4\sigma_{xy} \sin 2\theta - \{P_w + A(P_r - P_w)\} \tag{4.7}$$

$$\sigma_{zz} = \sigma_v - 2\vartheta(\sigma_x - \sigma_y) \cos 2\theta - 4\vartheta\sigma_{xy} \sin 2\theta - A(P_r - P_w) \tag{4.8}$$

$$\sigma_{\theta z} = 2(\sigma_{yz} \cos\theta - \sigma_{xz} \sin\theta) \tag{4.9}$$

Where:

θ	Is defined counter clockwise positive from the σ_{Hmax} direction in a vertical hole and from top in an inclined borehole
A	Poro-elastic constant: $A = \frac{(1-2\vartheta)\alpha}{1-\vartheta}$
α	Biot´s constant
P_r	Far-field reservoir pressure
ϑ	Poisson´s ratio
P_w	Wellbore pressure

In the case of an arbitrarily deviated well, the principle tangential effective stresses around the wellbore are given by:

$$\sigma_{tmax} = \frac{1}{2}(\sigma_{zz} + \sigma_{\theta\theta}) + \sqrt{(\sigma_{zz} - \sigma_{\theta\theta})^2 + 4\sigma_{\theta z}^2} \tag{4.10}$$

$$\sigma_{tmin} = \frac{1}{2}(\sigma_{zz} + \sigma_{\theta\theta}) - \sqrt{(\sigma_{zz} - \sigma_{\theta\theta})^2 + 4\sigma_{\theta z}^2} \tag{4.11}$$

The maximum effective tangential compressive stress around an arbitrarily oriented wellbore/perforation is found by solving the equation of the maximum tangential effective stresses, Eq.54, varying values of θ from 0 to 180° [23].

For a vertical well drilled parallel to the vertical principal stress, σ_v, the maximum and the minimum tangential compressive stress (Eq 4.10 and Eq 4.11) are given by the following equations:

$$\sigma_{tmax} = 3\sigma_x - \sigma_y - \{P_w + A(P_r - P_w)\} \quad (4.12)$$

$$\sigma_{tmin} = 3\sigma_y - \sigma_x - \{P_w + A(P_r - P_w)\} \quad (4.13)$$

4.2 Sand Failure Criterion

The source of the sand production is the presence of disintegrated sand grains around the wellbore or the perforation. Different mechanisms are responsible for the disintegration of the rock such as shear and tensile failure. In the developed sand prediction model, sand grains around the perforation or the borehole are assumed to disintegrate by shear failure when the maximum effective tangential compressive stress exceeds the effective strength formation as described by Willson et, all [24]:

$$\sigma_{tmax,eff} \geq U \quad (4.15)$$

Where

$$\sigma_{tmax,eff} = \sigma_{tmax} - \alpha P_w \quad (4.16)$$

$$U = 1.55 * Bf * TWC \quad (4.17)$$

$\sigma_{tmax,eff}$ the maximum effective tangential compressive stress

U the effective strength formation

σ_{tmax} the maximum tangential compressive stress

P_w Wellbore flowing pressure

α Biot´s constant $0 \leq \alpha \leq 1$

Bf Boost Factor

The boost factor is used to replicate the TWC strength value to provide more realistic formation strength resulting in more realistic failure prediction. A default BF of 2.5 is used for open-hole completions and 3.1 for cased and perforated completions due to the additional support provided by casing and cement as described by Willson [24].

The sand failure criterion (Eq 4.15) can be rewritten by considering the concept of the "Loading Factor", LF, as follows:

$$LF = \frac{\sigma_{tmax,eff}}{U} \geq 1 \tag{4.18}$$

This apparent sand failure criterion together with assuming linear-elastic behaviour can be used to estimate the onset of sanding by determining the critical bottom-hole flowing pressure resulting in sand production.

In this study field, the wells were assumed to be verticals, cased-and-perforated. In this case, the maximum tangential compressive stress around the perforation was determined based on Eq 4.12 and it, therefore, is expressed as follows:

$$\begin{aligned}\sigma_{tmax,eff} = 3\sigma_v - \sigma_{H\,max}\sin^2\alpha_{perf} - \sigma_{h\,min}\cos^2\alpha_{perf} \\ - \{P_w(1+\alpha) + A(P_r - P_w)\}\end{aligned} \tag{4.19}$$

Where

α_{perf} The angle between the perforation orientation and σ_{Hmax} direction. It is defined counter-clockwise positive from σ_{Hmax} direction

The model can accommodate the effect of the orientation of the perforation oriented at any deviation relative to the in-situ stress field which is reflected in the calculation of the maximum tangential compressive stress.

By rearranging the previous equation, Eq 4.19, the load factor around the perforation for the studied field can be expressed by:

$$LF = \frac{3\sigma_v - \sigma_{H\,max}\sin^2\alpha_{perf} - \sigma_{h\,min}\cos^2\alpha_{perf} - \{P_w(1+\alpha) + A(P_r - P_w)\}}{U} \tag{4.20}$$

By solving the inequality for P_w in the previous equation, (Eq. 4.20), the critical bottom-hole flowing pressure, CBHFP, resulting in sand production by perforation is expressed as follows:

$$CBHFP = \frac{3\sigma_v - \sigma_{H\,max}\sin^2\alpha_{perf} - \sigma_{h\,min}\cos^2\alpha_{perf} - U}{(1-\alpha-A)} - P_r\frac{A}{(1-\alpha-A)} \tag{4.21}$$

In many fields, sand production often does not occur at initial production conditions but it is triggered by depletion. This is normally a result of the increase in effective stresses caused by the decline of the reservoir pressure [1]. For a laterally large reservoir compared to its thickness, the change in vertical stress is considered negligible, thus it is usually kept

constant. The change in the maximum and minimum horizontal stresses is expressed as follows, respectively [23]:

$$\sigma_{H\,max} = \sigma_{H\,max} + A \times \Delta P \tag{4.22}$$

$$\sigma_{h\,min} = \sigma_{h\,min} + A \times \Delta P \tag{4.23}$$

Where

$$A = \frac{(1 - 2\vartheta)\alpha}{1 - \vartheta} \tag{4.24}$$

$$\Delta P = P_c - P_i \tag{4.25}$$

P_c Current reservoir pressure

P_i Initial reservoir pressure

4.3 Sanding Evaluation Workflow

Using the developed analytical solution, the computer program determines the critical pressure below which sanding is expected. The model requires as input data the geomechanical properties generated from the well log data and validated with drilling experiences and borehole conditions (figure 21). The methodology and assumptions considered in this model to calculate the geomechanical properties are described in chapter3.

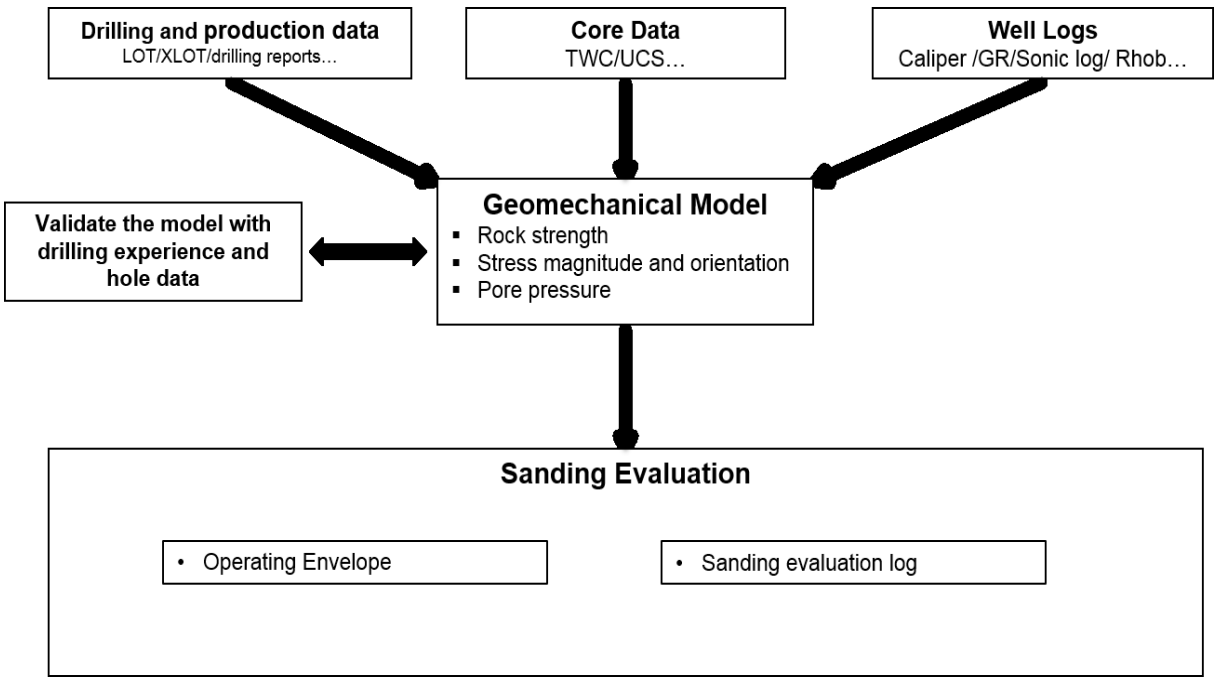

Figure 21: Sanding Evaluation Workflow

The results of the developed model consist of sand free operating envelopes and sanding evaluation log plots.

The sand free envelope is used to represent the critical bottom-hole pressure under various combinations of reservoir pressure and bottom hole flowing pressure. The plot axes, figure 22, are Bottom hole flowing pressure and the reservoir pressure. Above the blue line, the bottom hole flowing pressure is greater than the reservoir pressure, thus, no production is possible. The red line represents the sand failure threshold. Any combination of reservoir pressure and bottom hole flowing pressure falling below this threshold indicates that a failure condition has occurred for the relevant cavity (perforation/wellbore), and that sand production is assumed. For any combination of reservoir pressure and bottom hole flowing pressure falling above the same red line, there will be a no failure condition and sand-free production. Therefore, the zone between the red failure line and the blue line specifies the set of allowable drawdowns for sand free production [1].

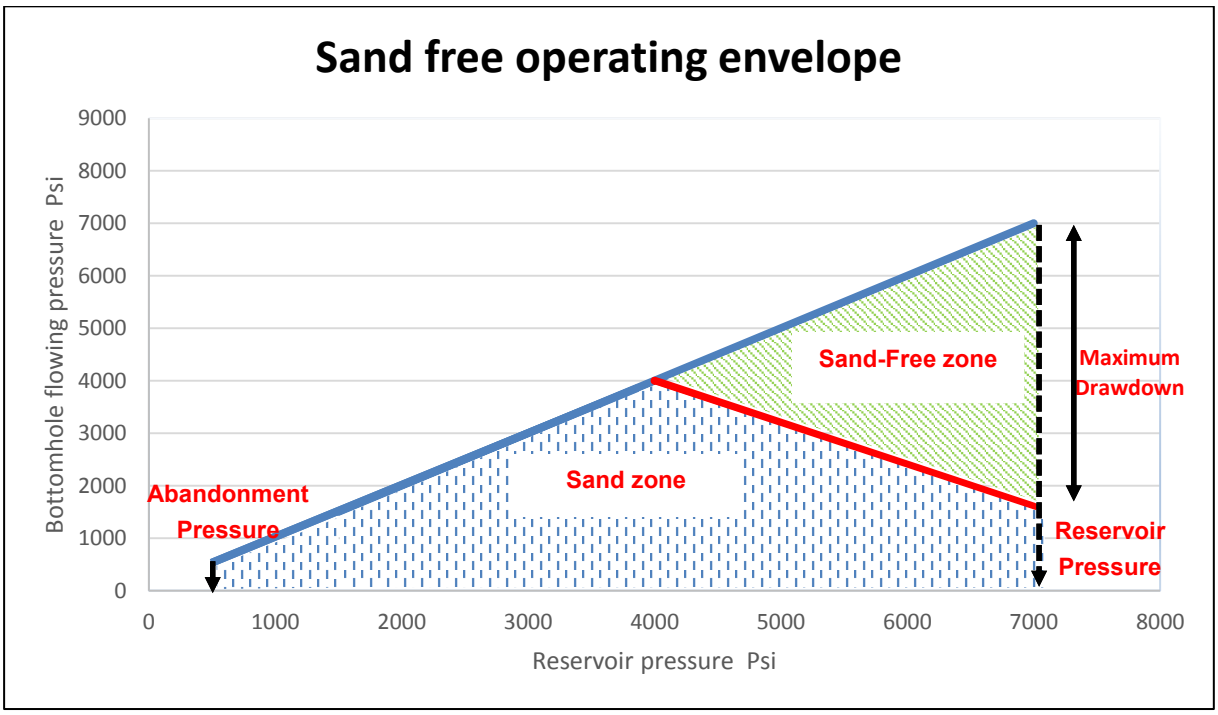

Figure 22: Generic Sand Free Operating Envelope

In the sanding evaluation log, the load factor and the critical drawdown pressure profiles are plotted over the entire reservoir section. The load factor represents the ratio of the maximum tangential effective compression stress to the effective stress of the formation. If the load factor is greater than 1 then the formation will fail and the sand production is assumed. For a given reservoir pressure, the critical drawdown is the difference between the reservoir pressure and the critical bottom hole flowing pressure. If the planned drawdown is higher than the critical drawdown then the formation will fail and the onset of the sand production is assumed [23].

4.4 Case Study

In order to test the model, it was essential to compare its results to the field observation. Therefore, the model was applied to three gas wells that have shown sand production during testing. The study wells were completed with a standard casing and perforations without sand control at the sand face.

Well-1 was drilled and completed in 2008. The well was completed with a selective single string completion consisting of 2 7/8" tail pipe, 2 hydraulic packers, 4 ½" production tubing and 3 SSDs to permit selective production. The well is cased and perforated in five sections from 3599.5 m TVD – 3874 m TVD. The reservoir targets of Well 1 are the "Acacus A" and "Tannezuft "sandstones.

Well-2 was drilled and completed in 2010. The well was completed with a single string completion consisting of 4 ½" production tubing, hydraulic packer, and a Tubing Retrievable Surface Controlled Subsurface safety valve (TRSCSSV). The well is cased and perforated in six sections from 3922.5 m TVD – 3961 m TVD. The reservoir targets of Well-2 are the "Acacus A" and "Tannezuft" sandstones.

Well-3 was drilled and completed in 2013. The well was completed with a single string completion consisting of 4 ½" tubing string, hydraulic packer, and a Tubing Retrievable Surface Controlled Subsurface safety valve (TRSCSSV). The well is cased and perforated in two sections from 4173 m TVD – 4198 m TVD. The reservoir targets of Well-3 are the "Acacus A" and "Tannezuft" sandstones.

5 Results and Discussion

This section presents the results of the sanding evaluation of the study wells generated by the analytical sand prediction model. The results are expressed in terms of sand free operating envelope. The sanding evaluation is run over the life-of-field operating condition from initial reservoir pressure to an arbitrary abandonment reservoir pressure of 600 psi. A Biot´s constant of 0.9 and Poisson´s ratio of 0.25 are used for effective stress and depletion calculation. A boost factor, BF, of 3.1 is used to replicate the TWC strength value to provide more realistic formation strength estimation.

As the field is associated with a normal-faulting regime and the study wells are vertical, the maximum horizontal stress direction is the worst for the perforation orientation in terms of sand production and the minimum horizontal stress direction is the best. This is because the perforation in the direction of the maximum horizontal stress direction becomes subject to the highest deviatoric stress$(\sigma_v - \sigma_{h\,\min})$. In this case, that the stress is orthogonal to the perforation axis resulting in perforation failure and hence the highest sanding risks [23]. Therefore, the sand risk is assessed for the best and the worst perforation orientation. In addition, the TWC strength of the wells at the perforation interval is determined using statistical analysis of the distribution of log derived strength values (see section 3.2.2). Therefore, three TWC strength case sensitivities are run for the sanding evaluation for each well (Table 6).

The sand free operating envelopes generated by the developed sand prediction model together with the results of the sand test were used to generate two valuable pieces of information for each well. First, the most realistic estimation of the formation strength was determined. Second, it is possible to evaluate the perforation orientation according to the best and worst direction for the most probable estimation of the formation strength case.

Table 6: TWC-Strength Sensitivities Cases

	TWC-Strength [psi]		
	P10	P50	P90
Well-1	5974	7860	8663
Well-2	6451	7543	8422
Well-3	5456	7302	8439

5.1 Well-1

The sanding evaluation for Well-1 was first conducted at the initial reservoir condition with an initial reservoir pressure of 6014 psi. Figures 23 through 25 are the sand free operating envelopes for Well-1 for the three TWC strength cases: P10, P50, and P90 respectively. The zone above the 45°slope line (blue line) in all operating envelopes is not considered in the interpretation as there is no sand production possible. The green and the red shaded zones represent the sand free production region for the best and the worst perforation orientation.

The sand production test of Well-1 indicated a significant sand production occurred at a drawdown pressure of 1000 psi. It can be seen that the sand free operating envelope shown in figure 23 is in agreement with the sanding test of Well-1.

Therefore, P10 TWC case was selected as the most probable formation strength estimation for Well-1. Based on figure 23, the conclusion that the perforation of Well-1 is oriented parallel to Shmax which corresponds to the worst direction. Under these conditions, it can be seen that Well-1 will experience sand production once the reservoir is depleted to 4800 psi as shown in figure 23.

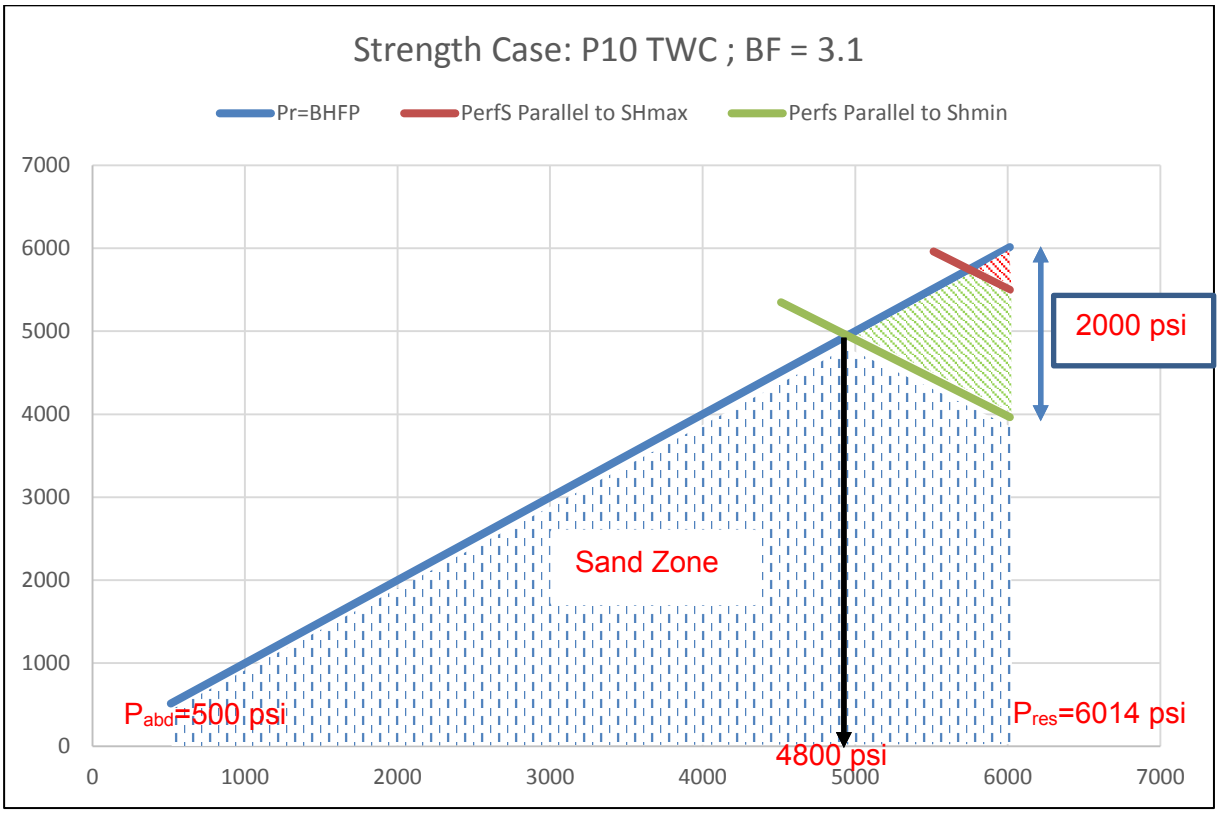

Figure 23: Sand-Free Operating Envelope of Well-1 for P10 TWC

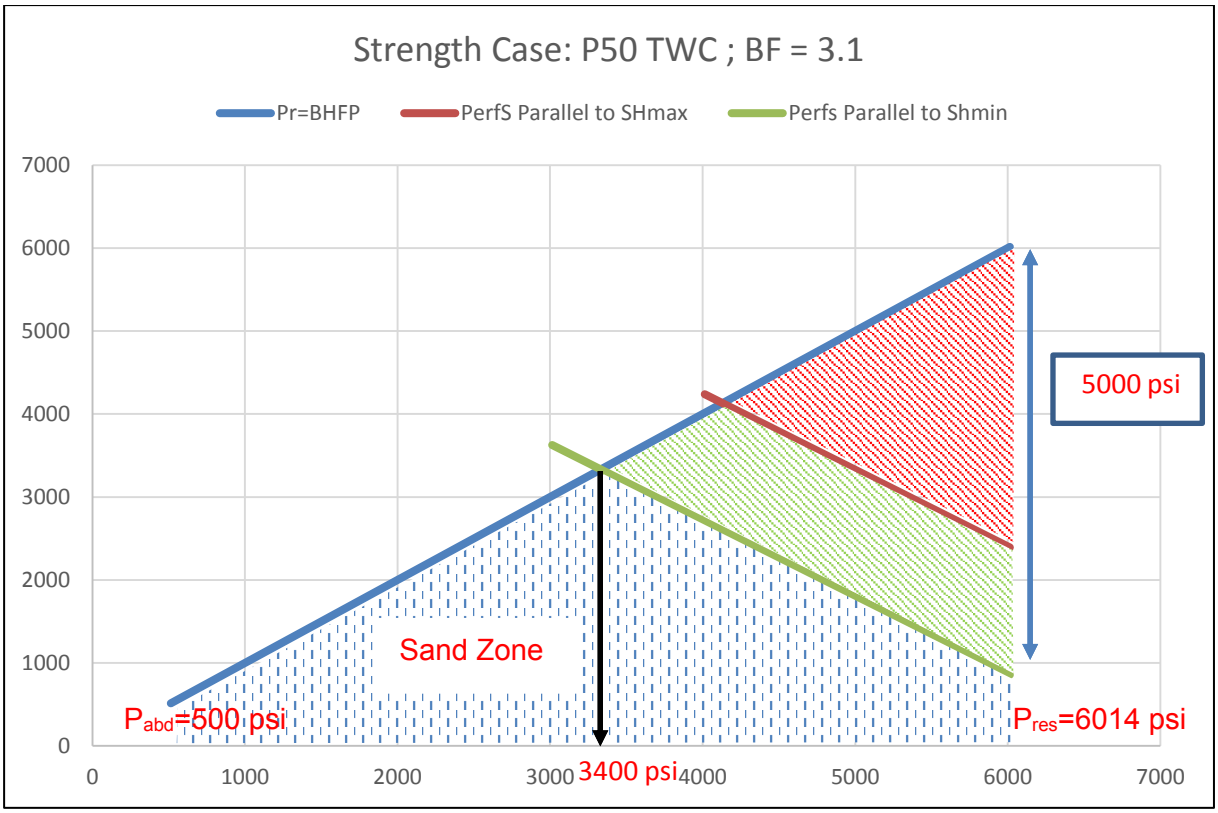

Figure 24: Sand-Free Operating Envelope of Well-1 for P50 TWC

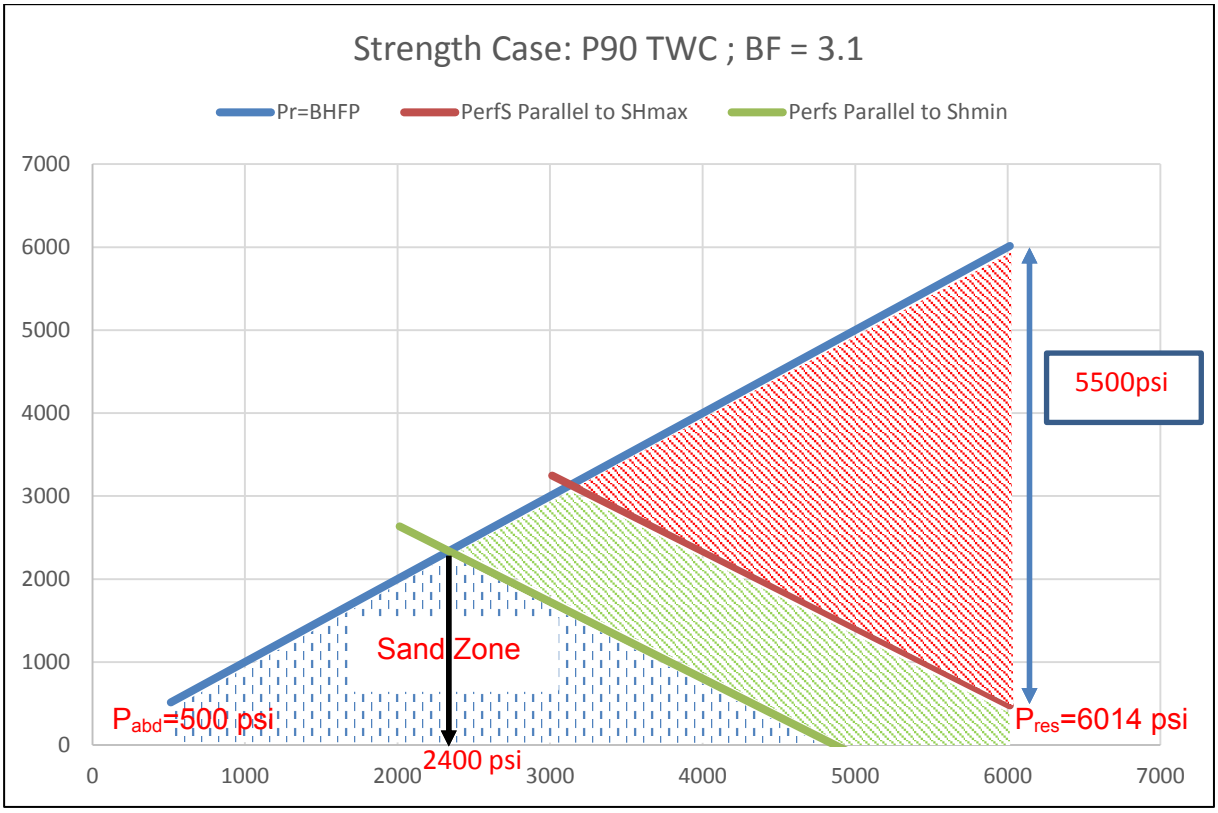

Figure 25: Sand-Free Operating Envelope of Well-1 for P90 TWC

5.2 Well-2

Similar to Well-1, the sanding evaluation for Well-2 is first conducted at the initial reservoir condition with an initial reservoir pressure of 6048 psi over the perforated section. Figures 26 through 28 are the sand free operating envelopes for Well-2 for the three TWC strength cases : P10, P50, and P90 respectively.

The sand production test of Well-2 shows a significant sand production occurred at a bottom-hole pressure of 4570 psi which is in agreement with the results of the analytical model generated for P10 TWC case. Therefore, P10 TWC case was selected as the most realistic formation strength estimation for Well-2.

Based on the sand free operating envelope for P10 TWC case, figure 26, we conclude that at initial reservoir condition, a drawdown of 1700 psi is possible before the onset of the sand production with the best perforation direction. Therefore, the perforations for Well-2 are orientated in the best direction. Under these conditions, it can be seen that Well-2 will experience sand production once the reservoir is depleted to 5200 psi as shown in figure 26.

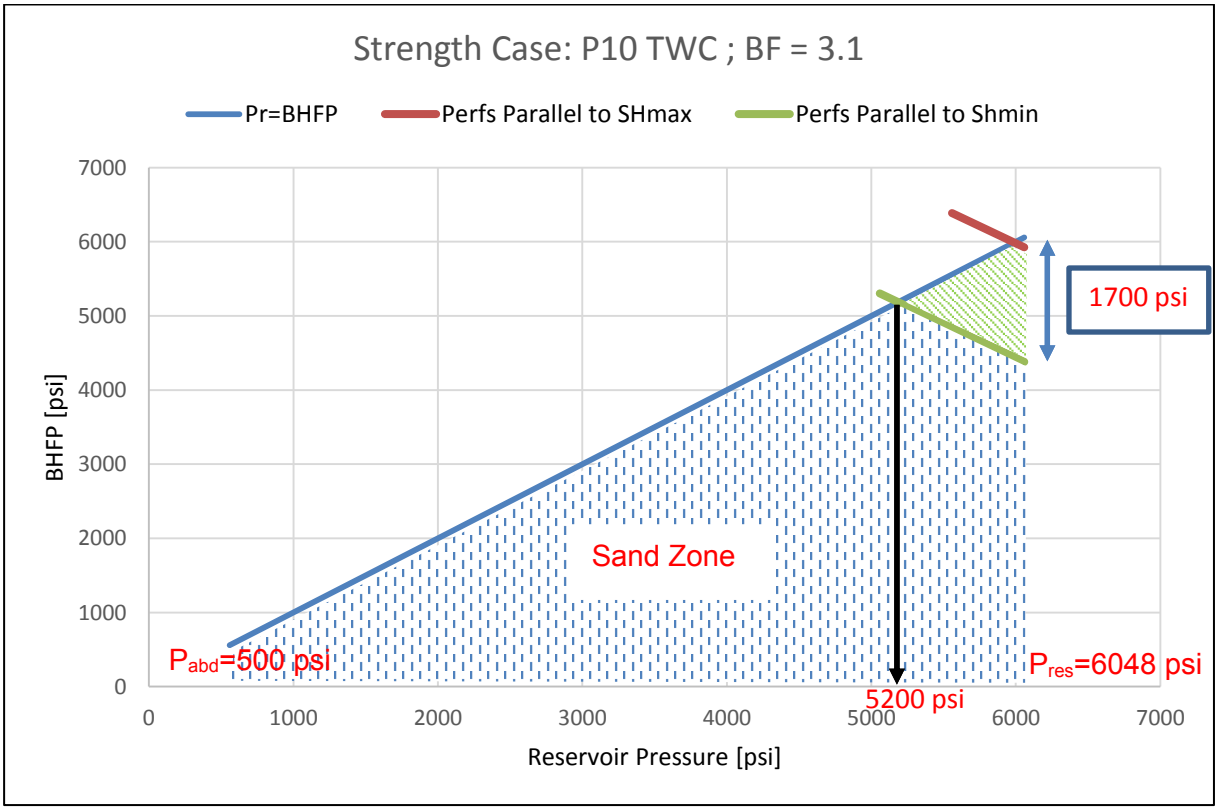

Figure 26: Sand-Free Operating Envelope of Well-2 for P10 TWC

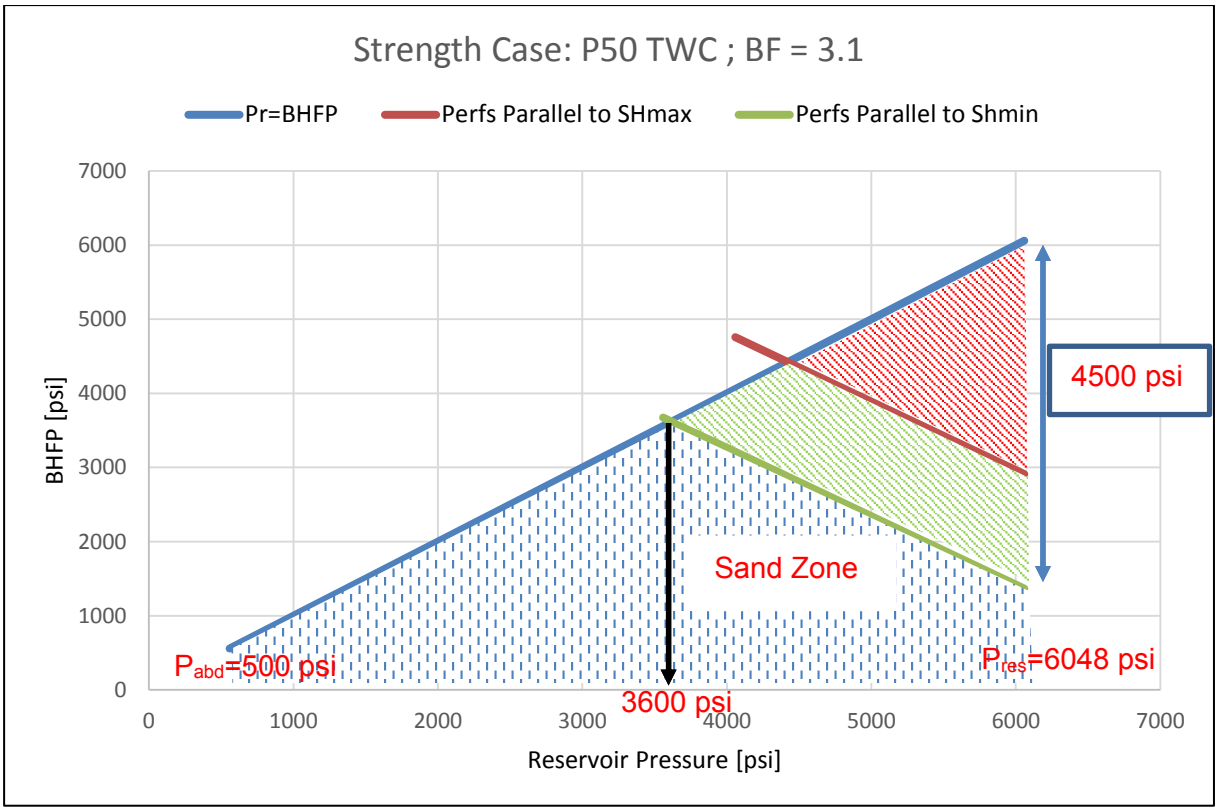

Figure 27: Sand-Free Operating Envelope of Well-2 for P50 TWC

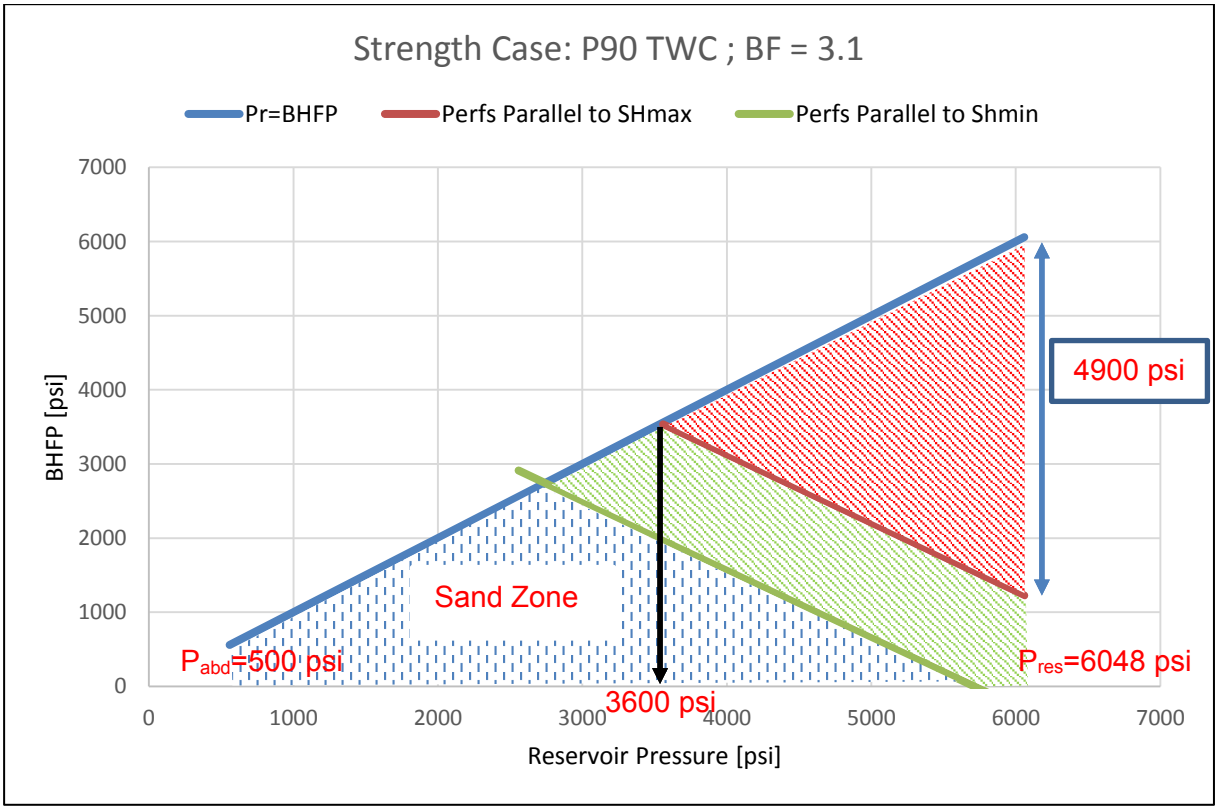

Figure 28: Sand-Free Operating Envelope of Well-2 for P90 TWC.

5.3 Well-3

The results of the sand production test for Well-3 indicate that a significant sand production occurs at bottom hole flowing pressure of 3722 psi at the initial reservoir pressure of 6014 psi. Figures 29 through 31 are the sand free operating envelopes for Well-3 for the three TWC strength cases: P10, P50 and P90 respectively.

Under P10 formation strength case, figure 29, it can be seen that Well-3 should experience sand production under initial reservoir condition for both worst and best perforation orientation. However, the sand free operation envelope generated for the P50 formation strength case is in agreement with the result of sand test for Well-3 as shown in figure 30. For the P90 formation strength, figure 31, a drawdown of 4000 psi is possible before the onset of the sand production with the worst perforation direction which is not consistent with the sand test of Well-3. Therefore, P50 TWC case was selected as the most realistic formation strength estimation for Well-3.

Considering the sand free operation envelope for the P50 strength case, figure 30, a drawdown of 2900 psi is possible before the onset of the sand production with the best perforation direction at the initial reservoir condition.

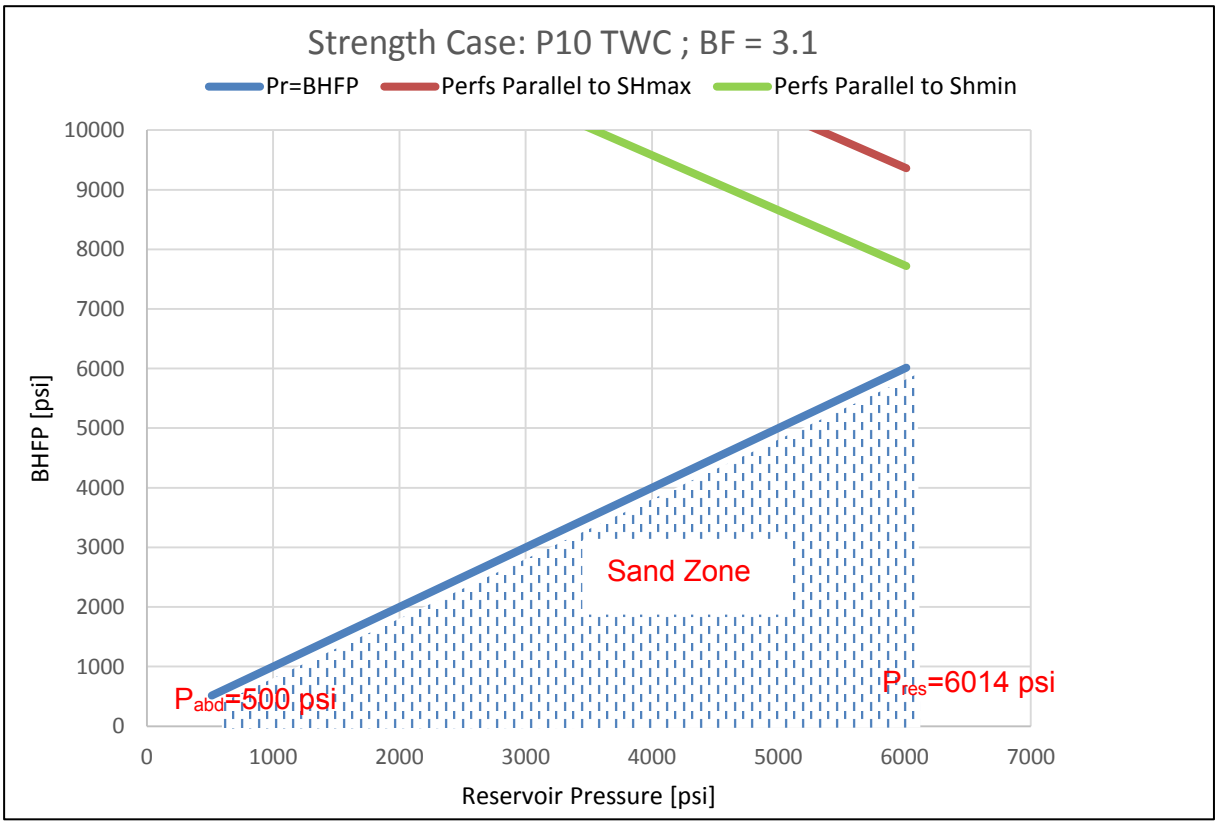

Figure 29: Sand-Free Operating Envelope of Well-3 for P10 TWC

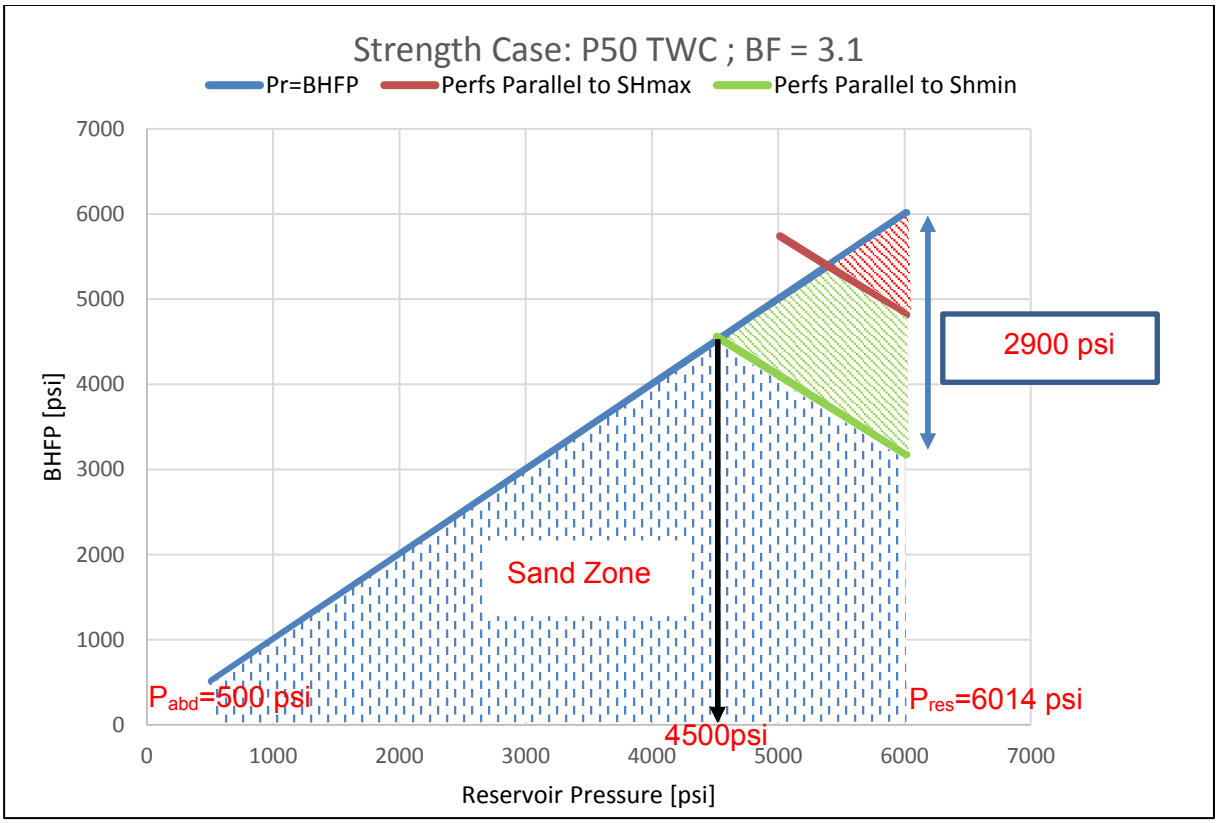

Figure 30: Sand-Free Operating Envelope of Well-3 for P50 TWC

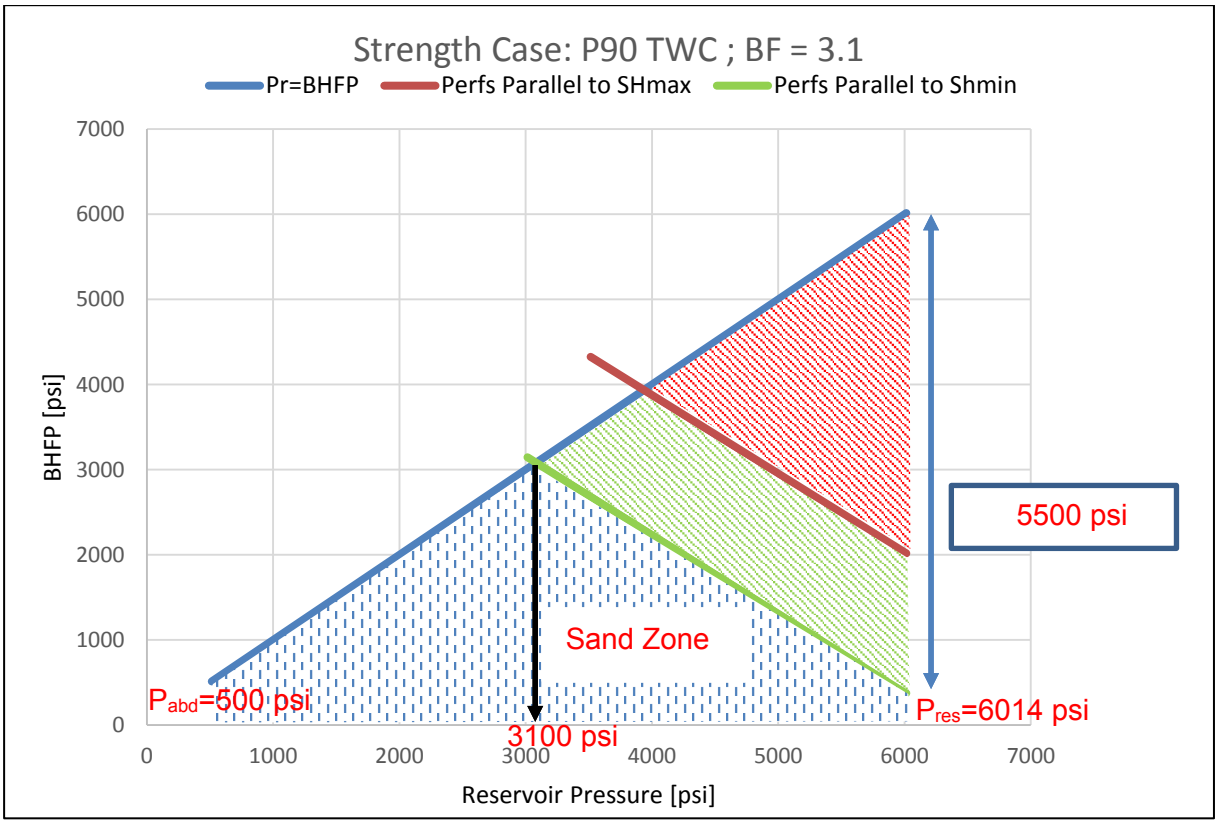

Figure 31: Sand-Free Operating Envelope of Well-3 for P90 TWC

6 Conclusions and Recommendations

In this thesis research, an analytical model was developed and explained to demonstrate the application of the well logs and failure criterion for prediction of sand production and calculation of critical wellbore pressure. Based on this research the following conclusions and recommendation for further research are summarized below.

6.1 Conclusions

1. An analytical model to predict sand production in a gas field has been developed. It can be used to estimate the critical bottomhole flowing pressure below which sanding is expected to occur. This model is based on the sand production criterion described by Wilson et al. [24], and utilizes the mechanical properties of the reservoir rock. The mechanical properties in the model are calculated from well-logging data. This makes the model a handy tool, allowing quick prediction of sand production and allows sand control decisions to be made at the time the well is logged and prior to completion.

2. A computer program that implements the model was developed using Microsoft Excel. The program was written in Visual Basic and provides a user-friendly interface.

3. The results of this model consist of sand free operating envelopes and sanding evaluation log plots. The results of the model provide two valuable pieces of information. First, the critical bottomhole pressure for each potential pay zone and second, the location of weak sand zones over the perforation intervals. Even if the predicted critical pressure values are not accurate for one reason or another, the relative formation strength of individual pay zones can be determined. This information can be used to avoid serious problems associated with sand production such as but not limited to wellbore instability, casing collapse and damage to the surface equipment.

4. The model was validated comparing results to actual field data gathered from three gas wells. The sanding evaluations results of the three wells generated by the analytical model were used to determine the most probable estimation of the formation strength and to evaluate the perforation orientation. It was concluded that the studied wells would experience sand production at an early stage of production. Therefore, sand control completions are recommended when producing from these wells.

6.2 Recommendations

1. In this thesis, the predictive accuracy of the developed sand prediction model was validated to actual field data gathered from three gas wells. In the future, it is necessary to calibrate the model to the sand production data gathered from all the wells in the field. In addition, it is recommended to use multiple failure criteria in predicting sand production and comparing the results from each criterion that could

provide more reliable estimates than using a single criterion. A parametric study is also recommended to investigate the effect of stress anisotropy, Poisson's ratio and Young's modulus on sand production prediction

2. The developed sand prediction model provides a technical support for sand control decision-making. Therefore, several problems associated with sand production can be avoided leading to lower intervention cost, hence the economic benefits of using the developed sand prediction model need to be investigated.

7 References

[1] OMV, "Reports".

[2] Balarabe, Tafida; Isehunwa, Sunday;, "Evaluation of sand production potential using well logs," *SPE-189107,* 2017.

[3] M. D. Zoback, Reservoir Geomechanics, 2010.

[4] Terzaghi, K; Peck, R B, Soil Mechanics in Engineering Practice, NewYork.

[5] Hall, D C; Harrisberger, H W, "Stability of Sand Arches: A Key to Sand Control," *JPT,* pp. 820-829, 1970.

[6] Cleary, M; Melvan, J; Kohlhass, A, "The Effect of Confining Stress and Fluid Properties on the Arch Stability in Unconsolidated sands," *SPE 8426,* 1979.

[7] Bratli, K; Risnes, R, "Stability and Failure of Sand Arches," *SPE 8427,* 1979.

[8] Stein, N; Hilchie, D.W;, "Estimating the Maximum Production Rate Possible from Friable Sandstones without Using Sand Control.," *Journal of Petroleum Technology 24 (9),* pp. 1157 - 1160, 1972.

[9] Tixier, M.P; Loveless, G.W; Anderson, R.A;, "Estimation of Formation Strength from the Mechanical-Properties Log," *Journal of Petroleum Technology 27 (3),* pp. 283 - 293, 1975.

[10] Peng, Suping; Zhang, Jincai;, Engineering Geology for Underground Rocks, NewYork, 2007.

[11] Sagrilo, Luis ; Castro Prates de Lima, Edison; Mendes de Sousa, Jose Renato; Volotão, Jane Vieira, "A Study on the Holding Capacity Safety Factors for Torpedo Anchors," *Applied Mathematics,* p. 18, 2012.

[12] Chen, X; Pang, S; Liu, Q, "Slope Stability Analysis Using Limit Equilibrium Method in Nonlinear Criterion," *Scientific World Journal,* p. 23 July 2014, 2014.

[13] Anderson, R A; Ingram, D S; Zanier, A M;, "Fracture pressure gradient determination from well logs," *Journal of Petroleum Technology,* pp. 1259-1268, 1973.

[14] Vicente , Brotons; Roberto , Tomás; Salvador , Ivorra; Angel, Grediaga;, "Relationship between static and dynamic elastic modulus of calcarenite heated at different

temperatures," *Bulletin of Engineering Geology and the Environment,* 2014.

[15] Zillur, Rahim; AL-Qahtani, Mohammed; Bartko, Kirk;, "The role of geomechanical earth modeling in the unconsolidated Pre-Khuff field completion design for saudi arabian gas wells," *SPE-84258,* 2003.

[16] Ewy, R.T; Ray, P; Bovberg, C.A. ; Goodman, H.E.; Norman, P.D;, "Openhole Stability and Sanding Predictions by 3D Extrapolation from Hole-Collapse Tests," *SPE-75328,* December 2001.

[17] Chang, C; Zoback, MD; Khaksar, A;, "Empirical relations between rock strength and physical properties in sedimentary rocks.," *Journal of Petroleum Science and Engineering,* vol. 51, pp. 223-237, 2006.

[18] Tranvoll, J; Morita, N; Santarelli, F;, "Perfoartion Cavity Stability: Comprehensive Laboratory Experiments and Numerical Analysis," *SPE 24799,* 1992.

[19] Fastwelltest, 2012. [Online]. Available: http://www.fekete.com/SAN/TheoryAndEquations/WellTestTheoryEquations/Fracture_Closure_Pressure.htm. [Accessed 19 11 2017].

[20] Breckels, I.M; Van Eckelen, H.A.M;, "Relationship Between Horizontal Stress and Depth in Sedimentary Basins," *SPE 10336,* September 1982.

[21] R. Ewy, "Wellbore-Stability Predictions by Use of a Modified Lade Criterion," *SPE 56862,* June 1999.

[22] Yi, X; Goodman, H.E; Williams, R.S; Hilarides, W.K;, "Building a Geomechanical Model For Kotabatak Field with Applications to Sanding Onset and Stability Predictions," *SPR-114697,* August 2008.

[23] Rahman , Khalil; Khaskar , Abbas; Kayes, Toby;, "An integrated Geomechanical and Passive Sand-Control Approach to Minimizing Sanding Risk From Openhole and cased and perforated Wells," *SPE-116633,* September 2008.

[24] Willson, S.M; Moschovidis, J.R; Palmer, I.D;, "New Model for Predicting the Rate of the Sand Prodcution," *SPE-78168,* 2002.

[25] Antheunis, D; Vriezen, B; Schipper, A; Van der Vlis, C;, "Perforation Collapse:Failure of Perforated Friable Sandstones," *SPE5750,* 1976.

[26] Morita, N; Whitfill, L; Fedde, P; Levik, H;, "Parametric Study of Sand Prodcution Prediction: Analytical Approach," *SPE16990,* 1987.

[27] Santarelli, J; Ouadfel , H; Zundel, P;, "Optimizing the completion Procedure to Minimize Sand Production Risk," *SPE 22797,* 1991.

[28] Tippie, B; Kohlhaas, A, "Effect of Flow Rate on Stability of Unconsolidated producing Sand," *SPE 4533,* 1973.

[29] Risnes, R; Bratli , K, "Sand Stress Around a Wellbore," *SPE9650,* 1981.

[30] Bradford, R; Cook, M;, "A semi-Analytic Elastoplastic Model for Wellbore Stability With Application to Sanding," *SPE/ISRM 28070,* 1994.

[31] Peden, J M; A.A.M, Yassine;, "The Determination of Optimum Completion and Production Conditions for Sand-Free Oil Production," *SPE 15406,* October 1986.

[32] Ong, Seehong; Zheng, Ziqiong;, "Sand production Prediction in high-rate, perforated and open-hole Gas Wells".

[33] Palmer, Ian; Vaziri, Hans; Willson, Stephen ; Moschovidis, Zissis; Cameron, John; Ispas, Ion;, "Predicting and Managing Sand Production: A New Strategy," *SPE-84499,* October 2003.

[34] K. Sung Hyun, "A Predictive Model for Sand Production in Poorly Consolidated Sands," 2010.

8 Appendices

8.1 Appendix-A: Geomechanical Properties Calculation File

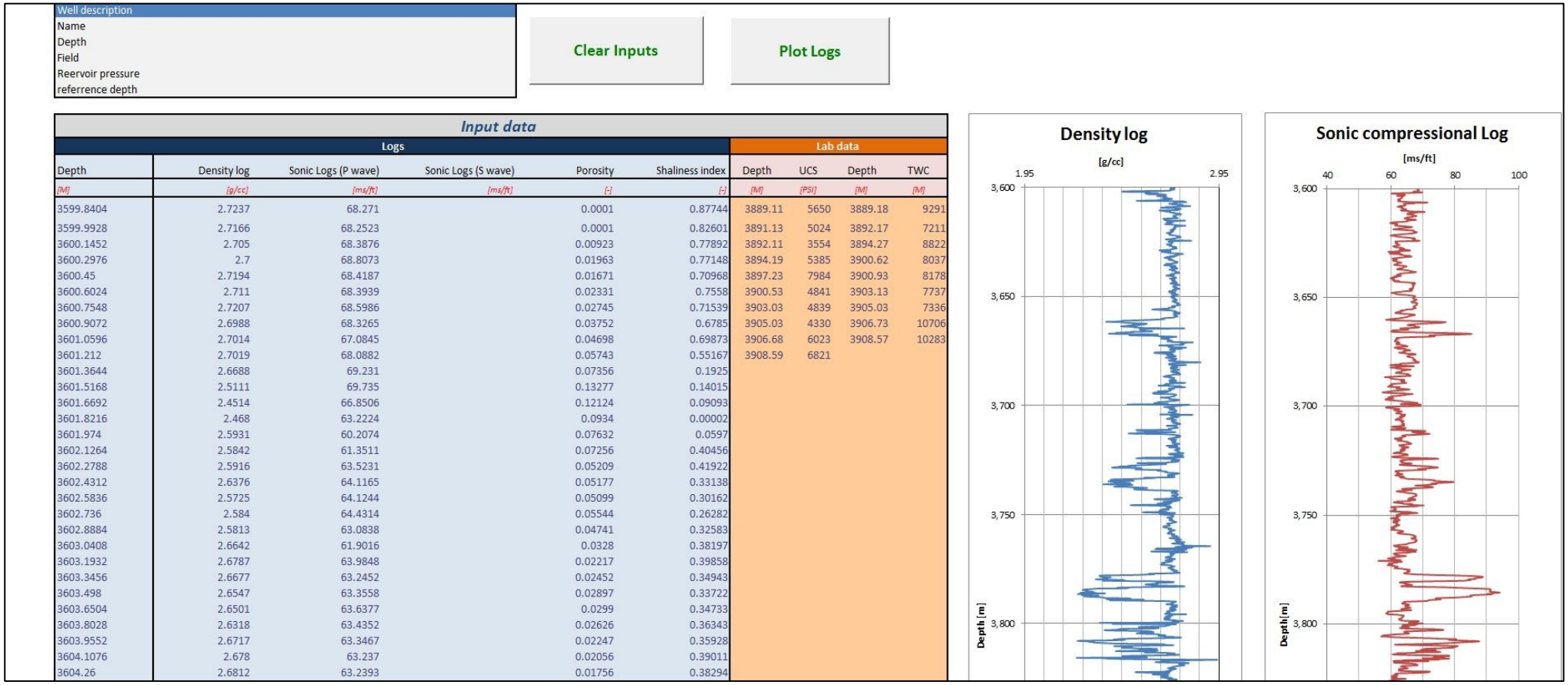

Well description
Name
Depth
Field
Reervoir pressure
referrence depth

Clear Inputs

Plot Logs

Input data

Logs						Lab data			
Depth	Density log	Sonic Logs (P wave)	Sonic Logs (S wave)	Porosity	Shaliness index	Depth	UCS	Depth	TWC
[M]	[g/cc]	[ms/ft]	[ms/ft]	[-]	[-]	[M]	[PSI]	[M]	[M]
3599.8404	2.7237	68.271		0.0001	0.87744	3889.11	5650	3889.18	9291
3599.9928	2.7166	68.2523		0.0001	0.82601	3891.13	5024	3892.17	7211
3600.1452	2.705	68.3876		0.00923	0.77892	3892.11	3554	3894.27	8822
3600.2976	2.7	68.8073		0.01963	0.77148	3894.19	5385	3900.62	8037
3600.45	2.7194	68.4187		0.01671	0.70968	3897.23	7984	3900.93	8178
3600.6024	2.711	68.3939		0.02331	0.7558	3900.53	4841	3903.13	7737
3600.7548	2.7207	68.5986		0.02745	0.71539	3903.03	4839	3905.03	7336
3600.9072	2.6988	68.3265		0.03752	0.6785	3905.03	4330	3906.73	10706
3601.0596	2.7014	67.0845		0.04698	0.69873	3906.68	6023	3908.57	10283
3601.212	2.7019	68.0882		0.05743	0.55167	3908.59	6821		
3601.3644	2.6688	69.231		0.07356	0.1925				
3601.5168	2.5111	69.735		0.13277	0.14015				
3601.6692	2.4514	66.8506		0.12124	0.09093				
3601.8216	2.468	63.2224		0.0934	0.00002				
3601.974	2.5931	60.2074		0.07632	0.0597				
3602.1264	2.5842	61.3511		0.07256	0.40456				
3602.2788	2.5916	63.5231		0.05209	0.41922				
3602.4312	2.6376	64.1165		0.05177	0.33138				
3602.5836	2.5725	64.1244		0.05099	0.30162				
3602.736	2.584	64.4314		0.05544	0.26282				
3602.8884	2.5813	63.0838		0.04741	0.32583				
3603.0408	2.6642	61.9016		0.0328	0.38197				
3603.1932	2.6787	63.9848		0.02217	0.39858				
3603.3456	2.6677	63.2452		0.02452	0.34943				
3603.498	2.6547	63.3558		0.02897	0.33722				
3603.6504	2.6501	63.6377		0.0299	0.34733				
3603.8028	2.6318	63.4352		0.02626	0.36343				
3603.9552	2.6717	63.3467		0.02247	0.35928				
3604.1076	2.678	63.237		0.02056	0.39011				
3604.26	2.6812	63.2393		0.01756	0.38294				

Figure 32: Input Data File

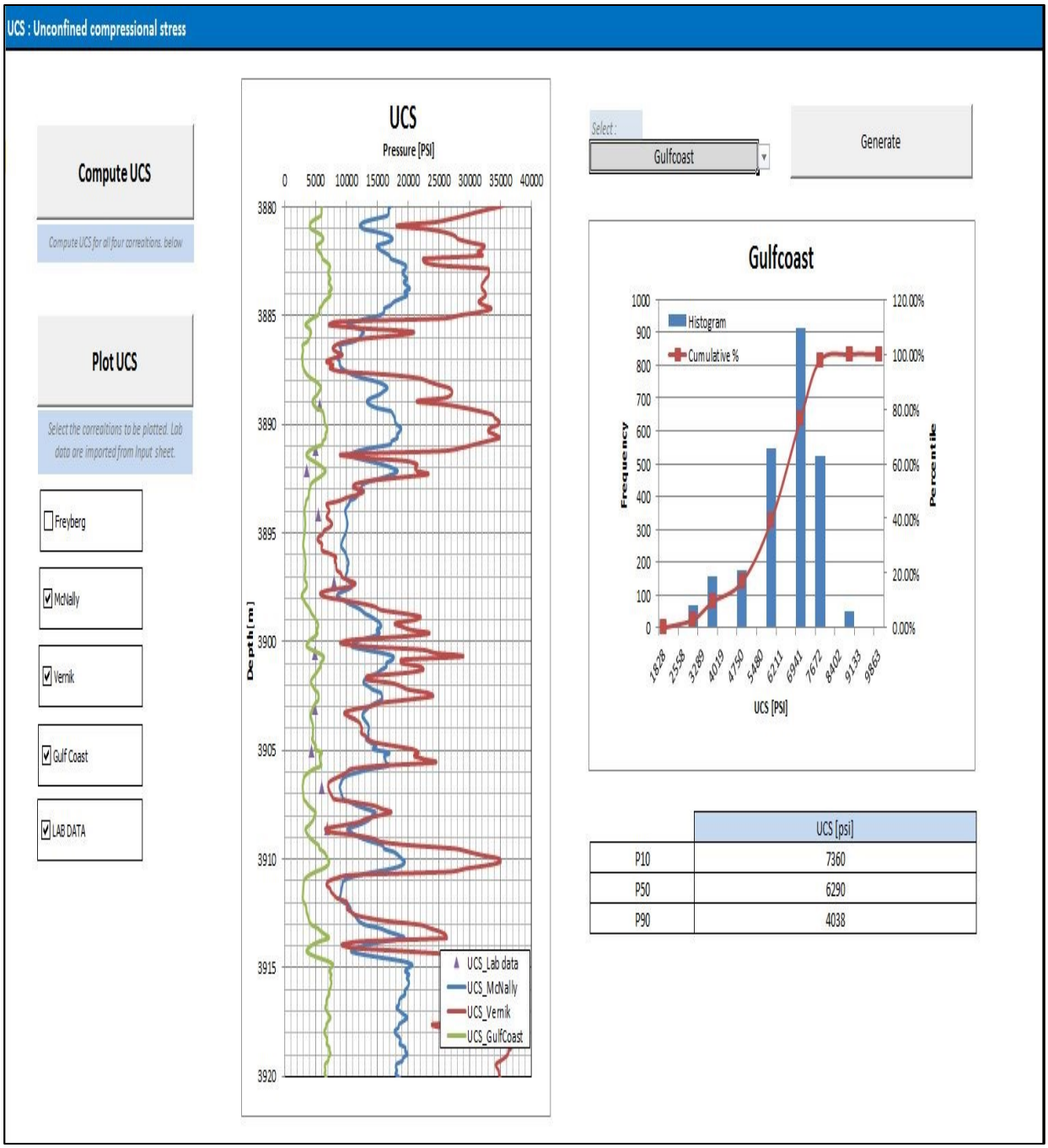

Figure 33: UCS-Generation from Well Log Data

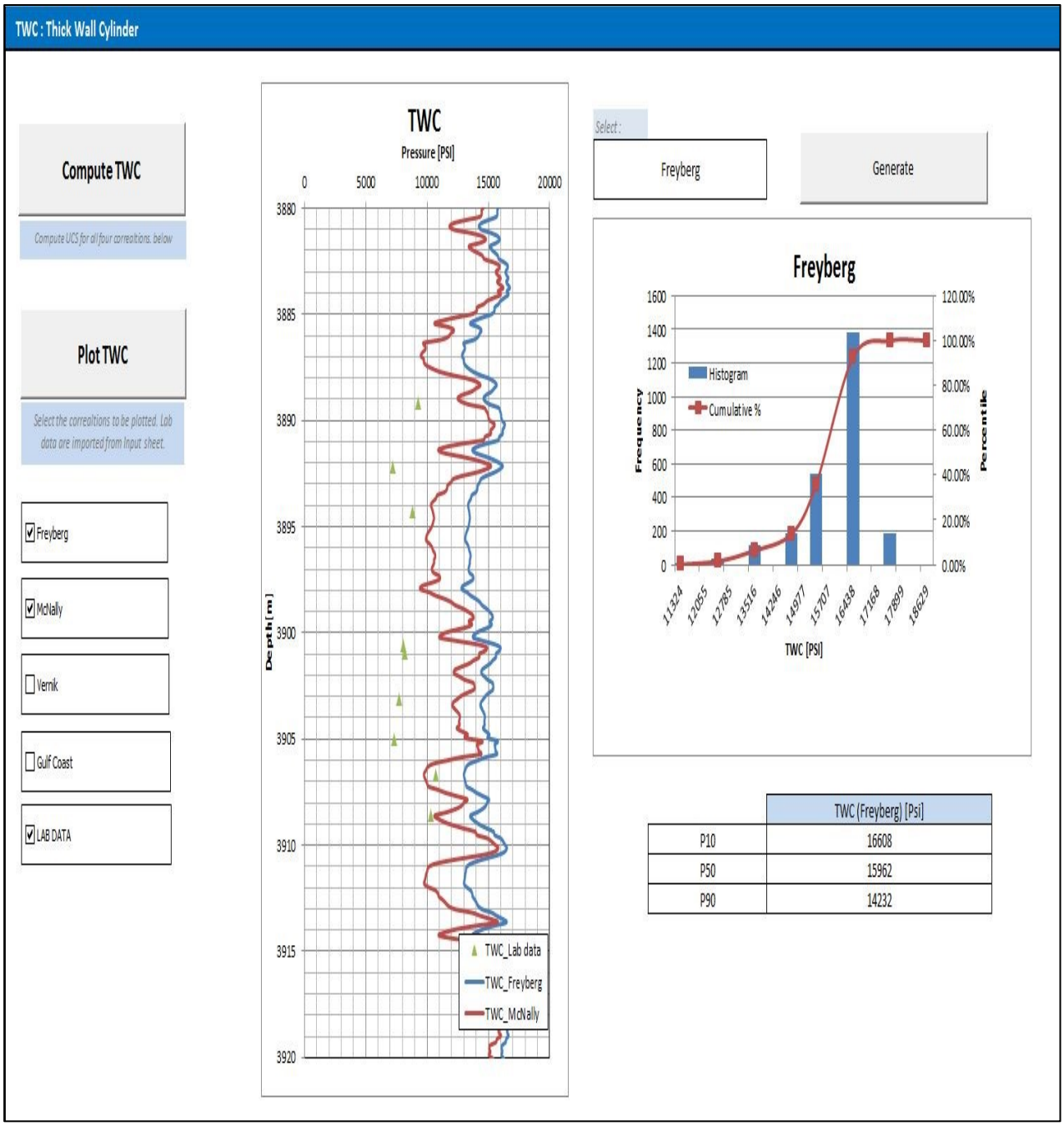

	TWC (Freyberg) [Psi]
P10	16608
P50	15962
P90	14232

Figure 34: TWC-Generation from Well Log Data

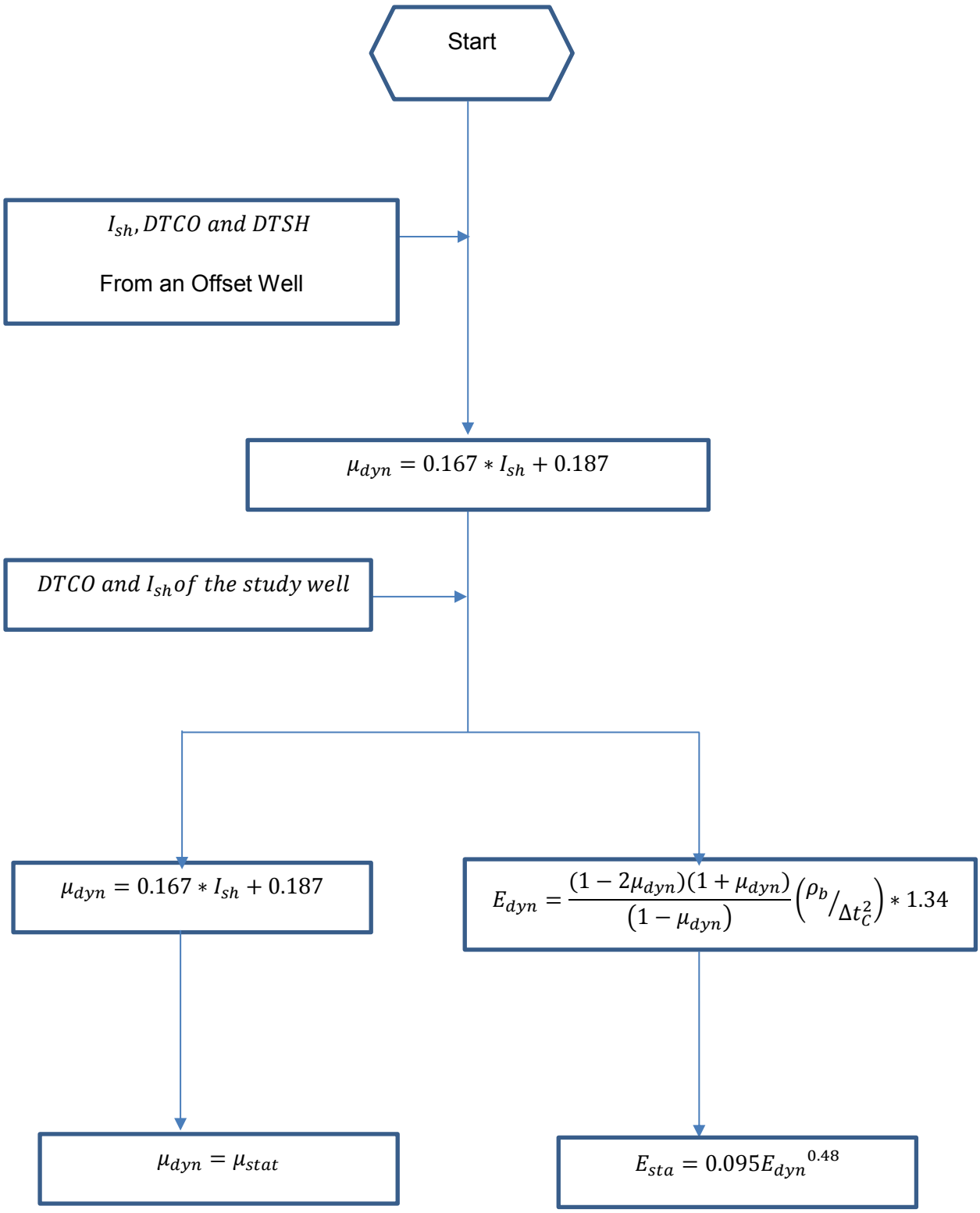

Figure 35: Flow Chart for Calculating Elastic Properties

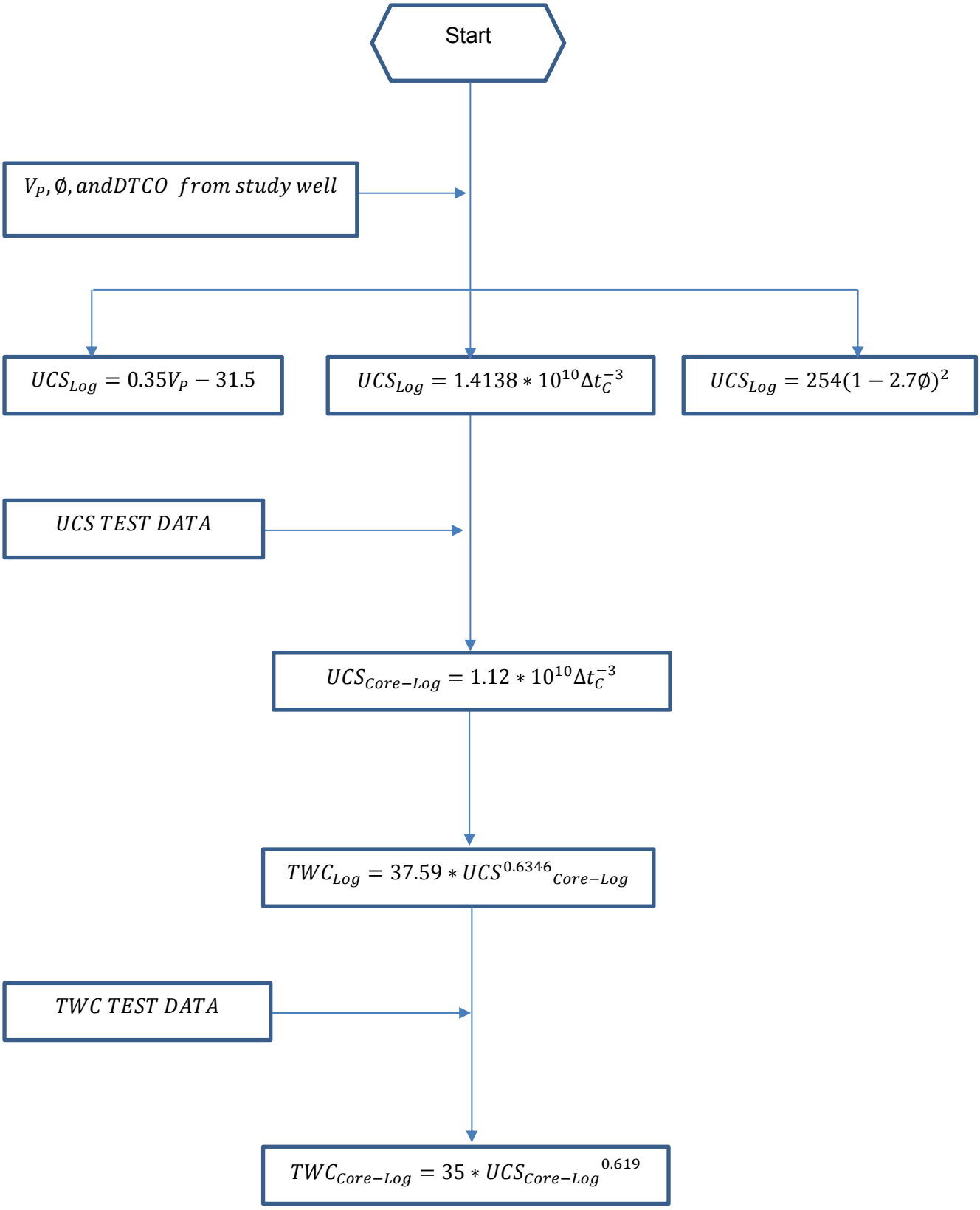

Figure 36: Flow Chart for Calculating Formation Strength Parameters

8.2 Appendix-B: Sanding Evaluation File

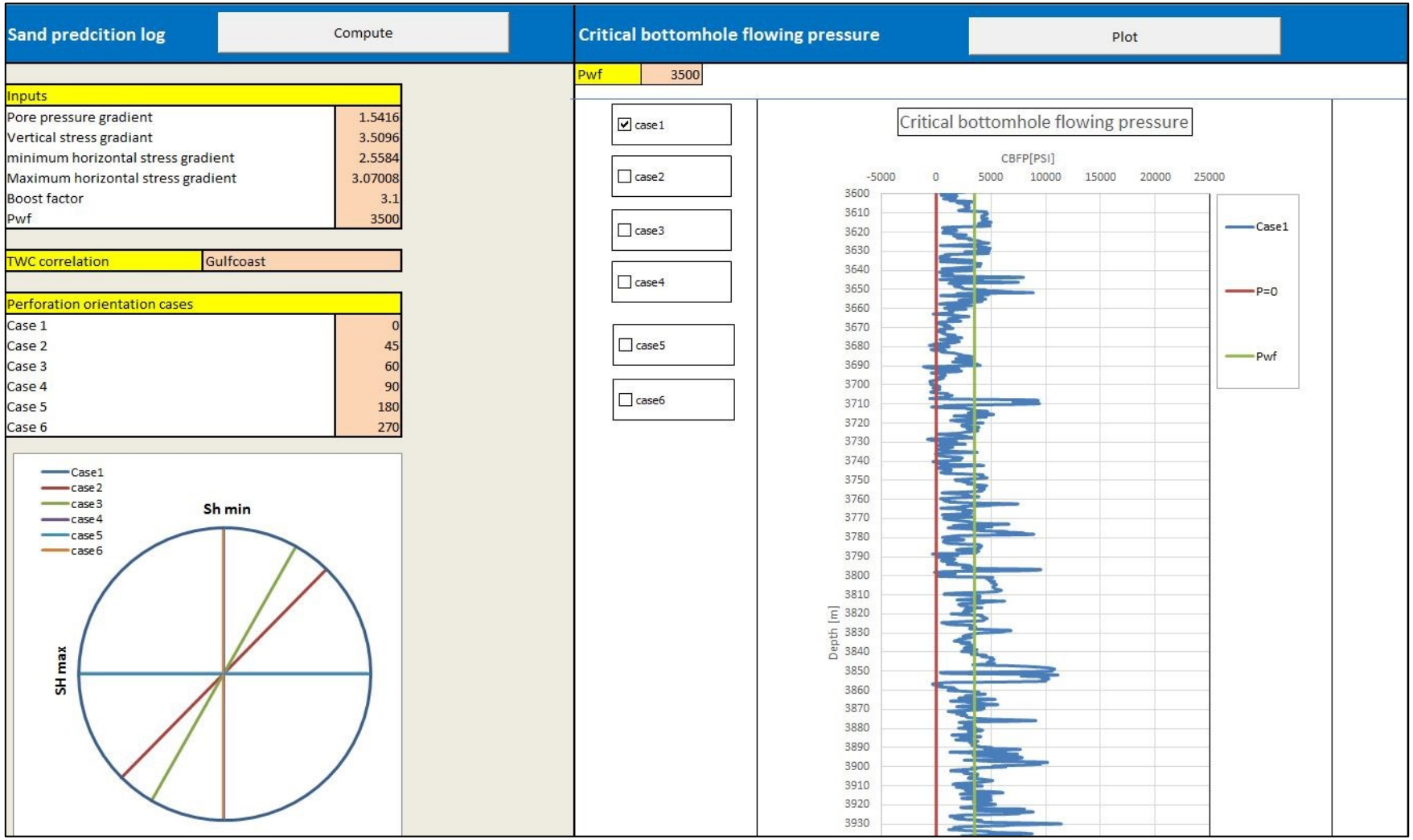

Figure 37: Sanding-Logs

Sand prediction Model

Import Data | Sand evaluating

Select TWC correlation	Gulfcoast
Select Evaluataion depth	3601.6692

Inputs

P10 TWC : 8663	
Pore pressure	5552.333239
Vertical stress	12640.41822
minimum horizontal stress	9214.510481
Maximum horizontal stress	11057.41258
Boost factor	3.1
Abandenment pressure *(tipe in)*	2000
Perforation orientation cases	
Case 1	0
Case 2	10
Case 3	20
Case 4	30
Case 5	40
Case 6	90

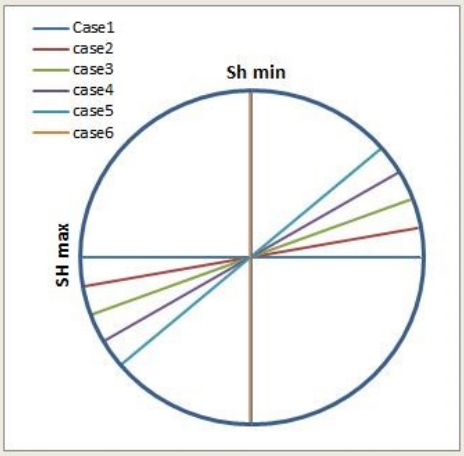

P50 TWC : 7860	
Pore pressure	5552.333239
Vertical stress gradiant	12640.41822
minimum horizontal stress gradient	9214.510481
Maximum horizontal stress gradient	11057.41258
Boost factor	3.1
Abandenment pressure *(tipe in)*	2000
Perforation orientation cases	
Case 1	0
Case 2	45
Case 3	60
Case 4	90
Case 5	180
Case 6	270

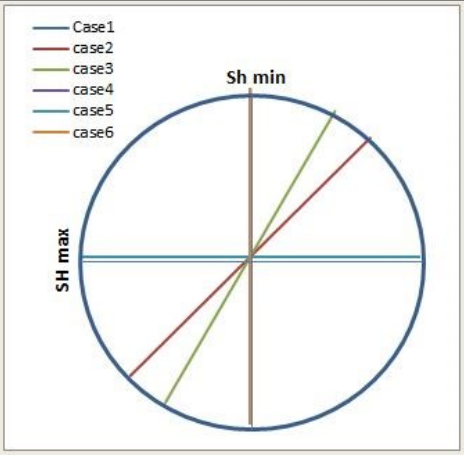

P90 TWC : 5974	
Pore pressure	5552.333239
Vertical stress gradiant	12640.41822
minimum horizontal stress gradient	9214.510481
Maximum horizontal stress gradient	11057.41258
Boost factor	3.1
Abandenment pressure *(tipe in)*	2000
Perforation orientation cases	
Case 1	0
Case 2	45
Case 3	60
Case 4	90
Case 5	180
Case 6	270

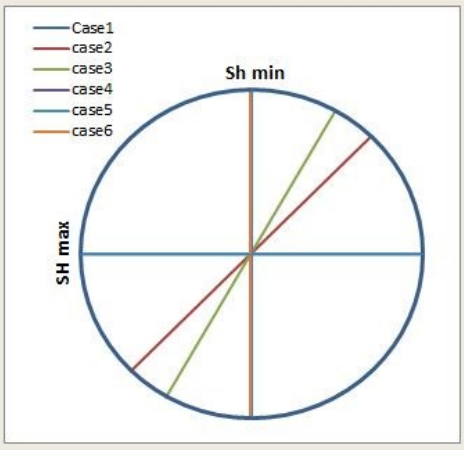

Figure 38: Sand-Free Operating Envelope Input File

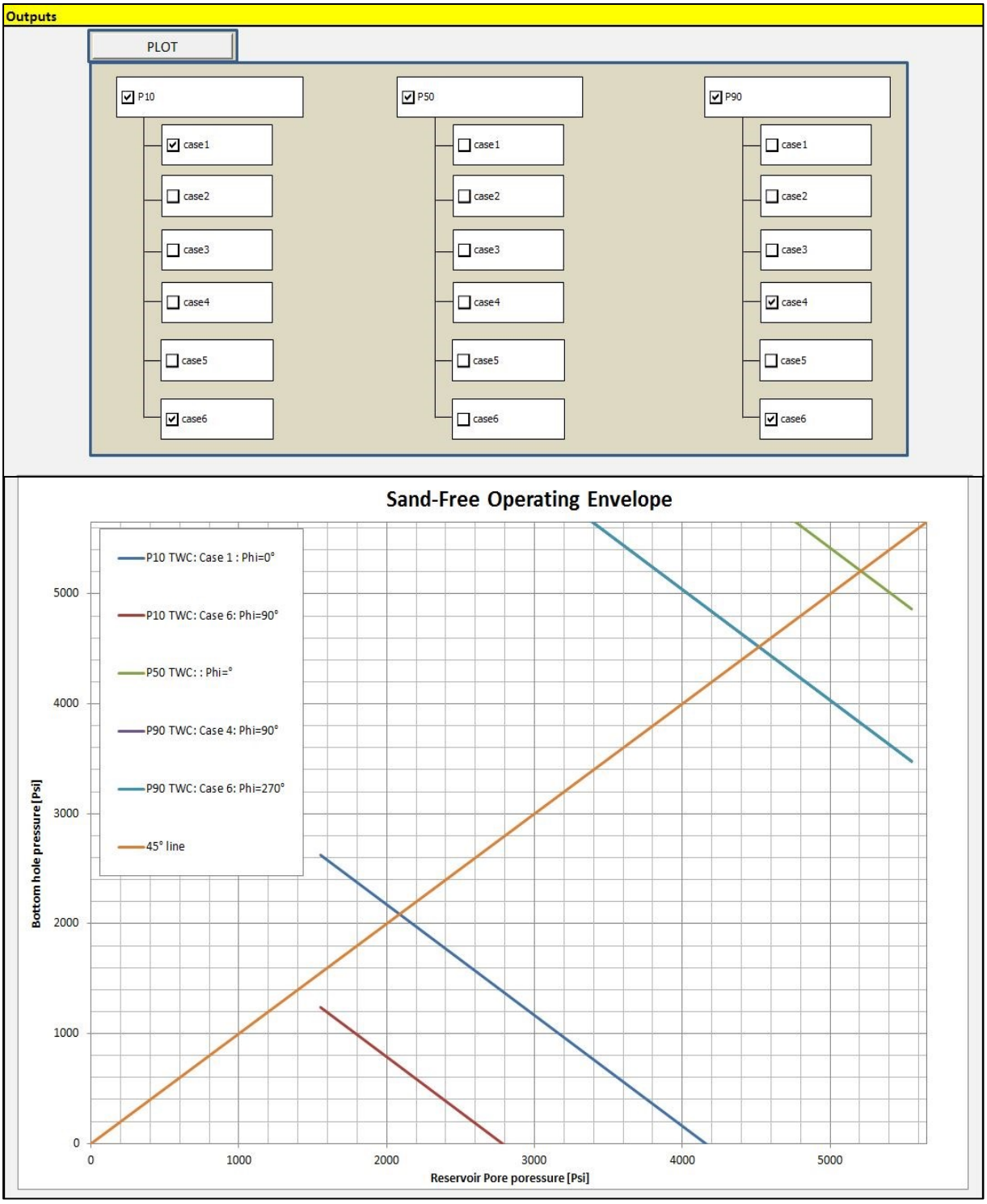

Figure 39: Sand-Free Operating Envelope

8.3 Appendix-C: Study Wells

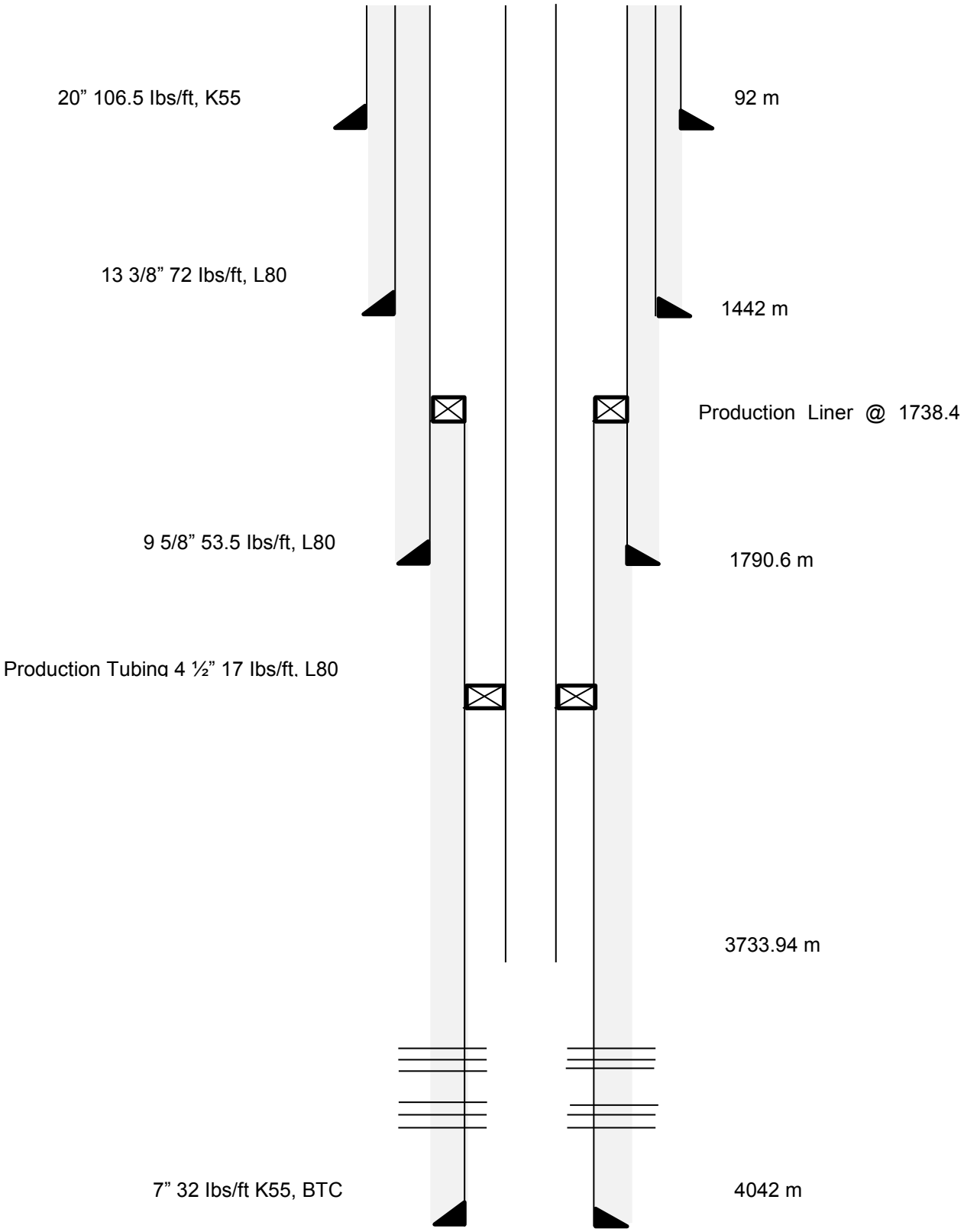

Figure 40: Completion Schematic of Well-1

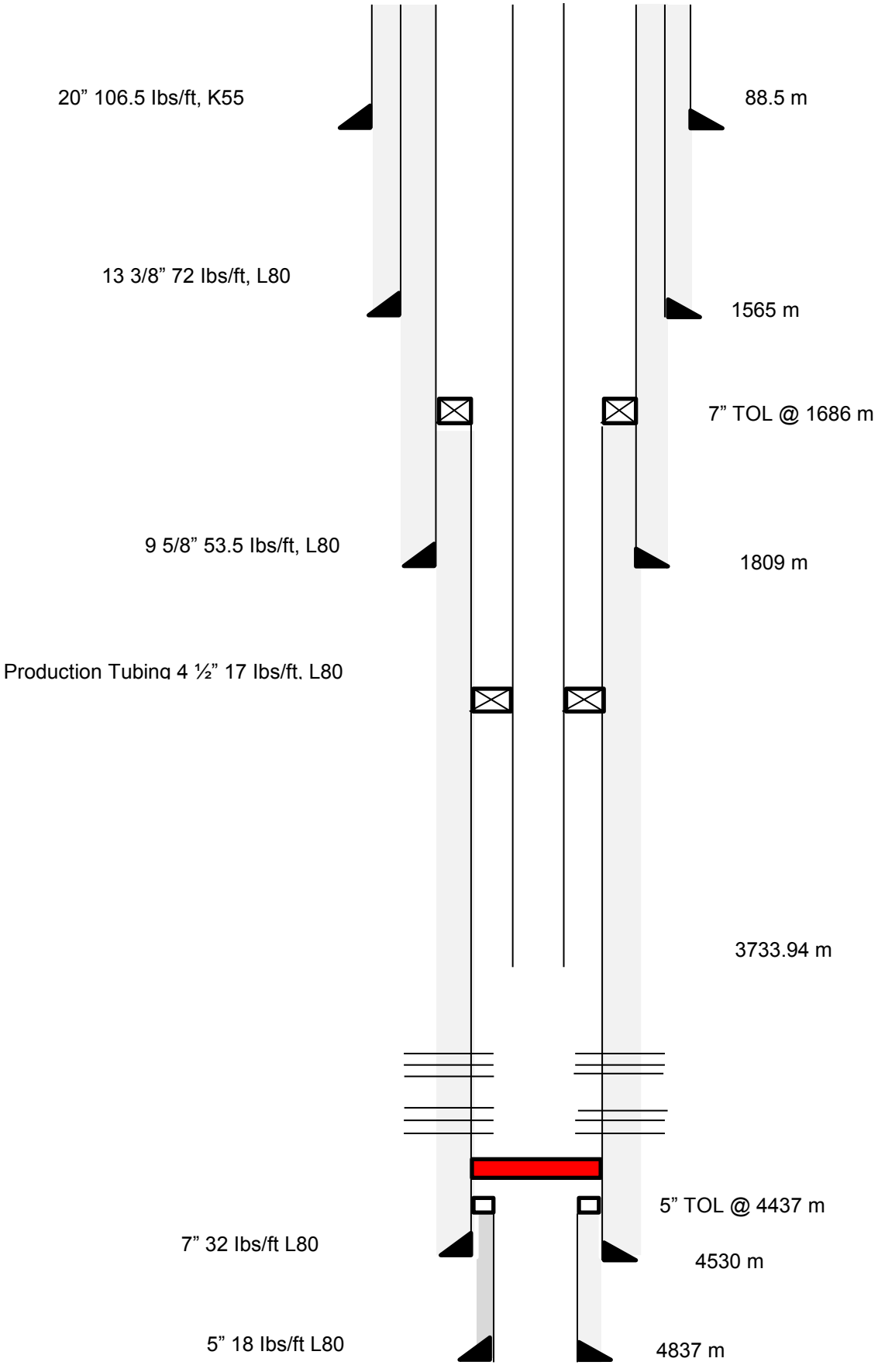

Figure 41: Completion Schematic of Well-2

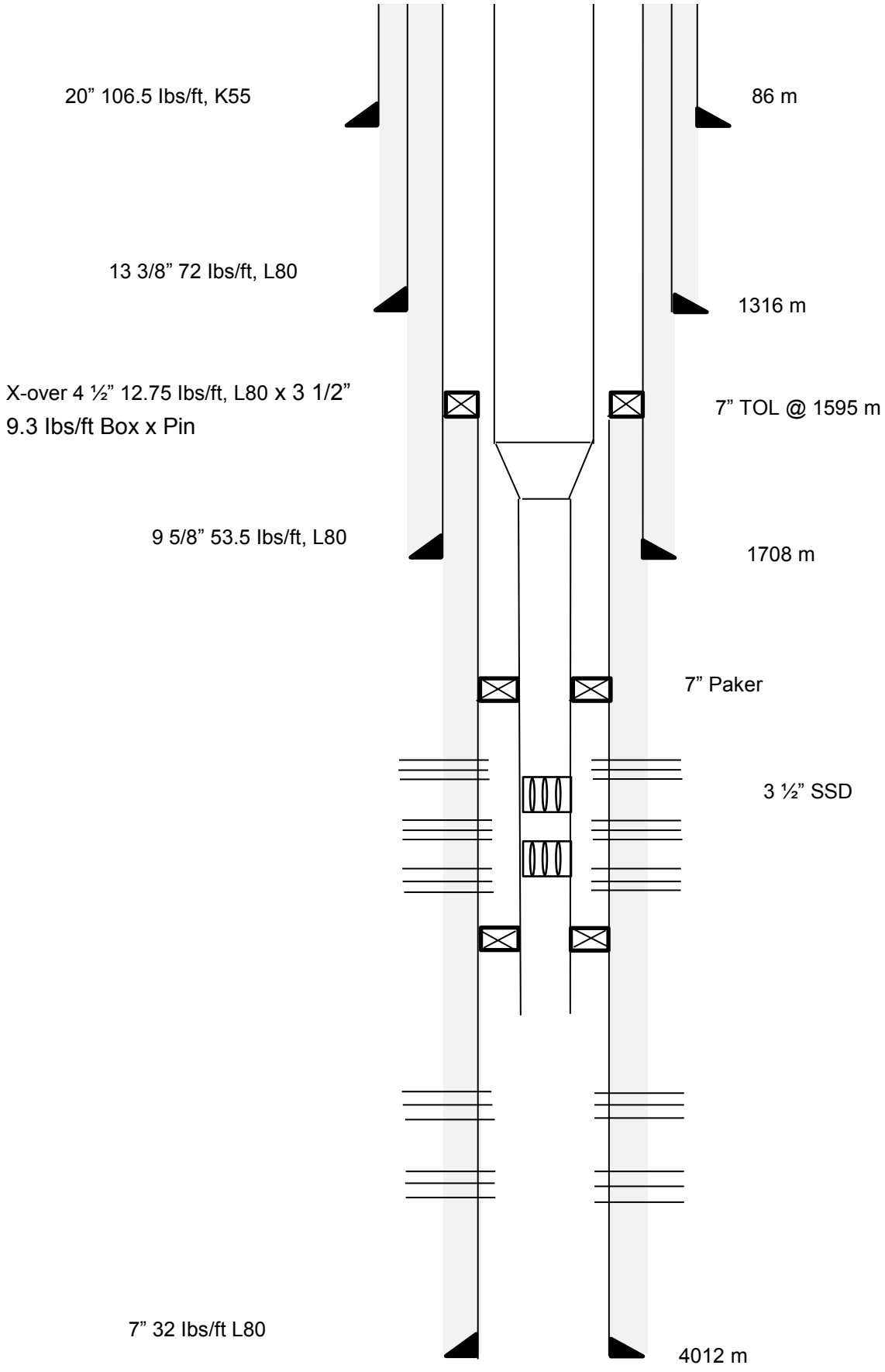

Figure 42: Completion Schematic of Well-3

Table 7: Unconfined Compressive Strength Results

Sample	Depth [m]	Length [mm]	Diameter [mm]	L: D	Saturated Bulk Density [g/cm3]	UCS [psi]
1	3889.11	50.89	24.88	2	2.33	5650
2	3891.13	50.66	25.15	2	2.38	5024
3	3892.11	50.86	24.92	2	2.30	3554
4	3894.19	50.92	25.02	2	2.32	5385
5	3897.23	50.84	25.10	2	2.41	7984
6	3900.53	50.81	24.97	2	2.28	4841
8	3902.25	50.89	25.24	2	2.39	10140
9	3903.03	50.80	24.96	2	2.24	4839
10	3905.03	51.03	24.94	2	2.26	4330
11	3906.68	51.81	25.05	2.1	2.31	6023
12	3908.59	50.99	25.08	2	2.30	6821

Table 8: Thick Walled Cylinder Results

Sample	Depth [m]	Length [mm]	OD [mm]	ID [mm]	SBD [g/cm3]	TWC Yield [psi]	TWC Collapse [psi]
1	3889.18	72.27	37.60	13.13	2.47	9090	9291
3	3892.17	76.14	37.62	13.13	2.31	6930	7211
4	3894.27	76.01	37.54	13.22	2.35	8630	8822
6	3900.62	76.27	37.52	13.23	2.30	7830	8037
7	3900.93	76.38	37.54	13.19	2.30	7940	8178
9	3903.13	75.88	37.41	13.37	2.28	7265	7737
10	3905.03	76.06	37.49	13.52	2.31	6980	7336
11	3906.73	76.18	37.74	13.17	2.42	10410	10706
12	3908.57	76.15	37.64	13.14	2.33	9330	10283